Accurate determination of $Fe^{3+}/\sum Fe$ of andesitic glass by Mössbauer spectroscopy

Revision 1

Hongluo L. Zhang[1*], Peat A. Solheid[2], Rebecca A. Lange[3], Anette von der Handt[1], Marc M. Hirschmann[1],

[1]Department of Earth Sciences, University of Minnesota, Minneapolis, MN 55455, USA

[2]Institute for Rock Magnetism, University of Minnesota, Minneapolis, MN 55455, USA

[3]Department of Earth and Environmental Sciences. University of Michigan, Ann Arbor, MI 48109, USA

Abstract

To evaluate the accuracy of Fe^{3+} and Fe^{2+} ratios in silicate glasses determined by Mössbauer spectroscopy, we examine in detail the temperature (47-293 K) of Mössbauer spectra for two andesitic glasses, one quenched at 1 atm, 1400 °C (VF3) and the other at 3.5 GPa, 1600 °C (M544). Variable-temperature Mössbauer spectra of these two glasses are used to characterize the recoilless fraction, *f*, by two different methods – a relative method (RM) based on the temperature dependence of the ratios of Fe^{3+} and Fe^{2+} Mössbauer doublets and the second based on the temperature dependence of the center shift (CS) of the doublets. The ratio of the recoilless fractions for Fe^{3+} and Fe^{2+}, C_T, can then be used to adjust the observed area of the Mössbauer doublets into the $Fe^{3+}/\Sigma Fe$ ratio in the sample. We also evaluated the

contributions of non-paramagnetic components to the Fe in the glasses by determining the influence of applied magnetic field on sample magnetization. Finally, for the VF3 glass, we determined the $Fe^{3+}/\Sigma Fe$ independently by wet chemical determination of the FeO content combined with careful electron microprobe analyses of total Fe. Recoilless fractions determined with the CS method (CSM) are significantly smaller than those determined with the relative method and suggest larger corrections to room temperature $Fe^{3+}/\Sigma Fe$ ratios. However, the RM determinations are believed to be more accurate because they depend less on the assumption of the Debye harmonic model and because they produce more nearly temperature-independent estimates of $Fe^{3+}/\Sigma Fe$ ratios. Non-linear responses of sample magnetizations to applied magnetic fields indicate that the glasses contain a small (0.4-1.1 % for VF3) superparamagnetic component that is most likely to be nanophase precipitates of $(Fe,Mg)Fe_2O_4$ oxide, but corrections for this component have negligible influence on the total $Fe^{3+}/\Sigma Fe$ determined for the glass. For the VF3 glass, the $Fe^{3+}/\Sigma Fe$ produced by uncorrected room temperature Mössbauer spectroscopy (0.685±0.014 in two standard deviation (2σ)) agrees within 3% of that determined by wet chemistry (0.666±0.030 in 2σ). The $Fe^{3+}/\Sigma Fe$ corrected for recoilless fraction contributions is 0.634±0.078(2σ), which is 7.5% lower than the uncorrected room temperature ratio, but also agrees within 5% of wet chemical ratio. At least for this andesitic glass, the room temperature determination of $Fe^{3+}/\Sigma Fe$ is accurate within analytical uncertainty, but room temperature Mössbauer determinations of $Fe^{3+}/\Sigma Fe$

are always systematically higher compared to recoilless-fraction corrected ratios.

1 Introduction

The proportion of Fe^{3+} and Fe^{2+} in natural and experimental silicate glasses is one of the most important measures of the oxygen fugacity of magmatic materials, and consequently has been the subject of intensive study for more than 30 years (Sack et al., 1981; Mysen et al., 1985; Christie et al., 1986; Mysen and Virgo, 1986; Carmichael and Kress, 1988; Jayasuriya et al., 2004; Bézos and Humler, 2005; O'Neill et al., 2006; Wilke et al., 2006; Rossano et al., 2008; Cottrell et al., 2009; Kelley and Cottrell, 2009; Cottrell and Kelley, 2011; Cottrell and Kelley, 2013). Analytical techniques employed to determine $Fe^{3+}/\Sigma Fe$ in silicate glasses include wet chemistry (Wilson, 1960; Sack et al., 1981; Mysen et al., 1985; Christie et al., 1986; Carmichael and Kress, 1991; Bézos and Humler, 2005), and, increasingly, XANES (Wilke et al., 2001; Berry et al., 2008; Cottrell et al., 2009; Kelley and Cottrell, 2009; Cottrell and Kelley, 2011; Cottrell and Kelley, 2013), but the most commonly applied technique is Mössbauer spectroscopy (Mysen et al., 1985; Mysen and Virgo, 1985; Mysen and Virgo, 1986; Dyar et al., 1987; Dingwell, 1991; Jayasuriya et al., 2004; O'Neill et al., 2006; Rossano et al., 2008; Cottrell et al., 2009; Borisov and McCammon, 2010; Righter et al., 2013). However, some controversy has persisted about the relative accuracies of these different techniques, and in particular, about the veracity of $Fe^{3+}/\Sigma Fe$ determined by Mössbauer spectroscopy (Lange and Carmichael, 1989; Ottonello et al., 2001; Righter et al., 2013).

Recoilless interactions between ^{57}Co 14.4 keV gamma quanta and the nuclei of $^{57}Fe^{3+}$ and $^{57}Fe^{2+}$ ions occur at distinct energies and produce significant separation in Doppler-shifted velocities, potentially allowing precise quantification of $Fe^{3+}/\Sigma Fe$ in Fe-bearing materials, including silicate glasses (McCammon and Kopylova, 2004). However, the accuracy of such determinations depends on corrections for several effects. The most important is the relative proportion of recoilless fractions of Fe^{3+} and Fe^{2+} ions, ($f(Fe^{3+})_T$, $f(Fe^{2+})_T$), which represent the temperature-dependent fractions of 14.4 keV gamma rays interacting resonantly with the $^{57}Fe^{3+}$ and $^{57}Fe^{2+}$ ions. The absorption areas of Mössbauer doublets produced by Fe^{3+} and Fe^{2+} in an analyte ($AA(Fe^{3+})_T$, $AA(Fe^{2+})_T$) are related to the abundances of the ions ($N(Fe^{3+})_T$, $N(Fe^{2+})_T$) and the recoilless fraction of each ion, according to

$$\frac{AA\left(\mathrm{Fe}^{3+}\right)_T}{AA\left(\mathrm{Fe}^{2+}\right)_T} = C_T \frac{N\left(\mathrm{Fe}^{3+}\right)}{N\left(\mathrm{Fe}^{2+}\right)} \qquad (1)$$

where C_T is correction number, equals $f(Fe^{3+})_T/f(Fe^{2+})_T$, and the T subscripts highlight quantities that are temperature-dependent. As the recoilless interaction depends on bond strength and is affected by lattice vibrations (Chen and Yang, 2007), values of f_T are usually not the same for Fe^{3+} and Fe^{2+} in minerals or glasses. Indeed, studies of silicate and oxide minerals have found values of C_T at room temperature ranging from 1.0 in biotite (Bancroft and Brown, 1975) to 1.4 in garnet (Woodland and Ross II, 1994; Dyar et al., 2012), but typical values average near 1.2 (De Grave and Van Alboom, 1991).

Despite the demonstrated importance of recoilless fractions for $Fe^{3+}/\Sigma Fe$ determinations in silicate minerals, Mössbauer analyses of $Fe^{3+}/\Sigma Fe$ in silicate glasses are commonly conducted at room temperature without correction for recoil-free effects (Mysen et al., 1985; Dyar et al., 1987; Dingwell, 1991; Jayasuriya et al., 2004; O'Neill et al., 2006; Rossano et al., 2008; Cottrell et al., 2009; Borisov and McCammon, 2010). This simplification may be justified because some comparisons between uncorrected room temperature Mössbauer measurements and $Fe^{3+}/\Sigma Fe$ determined by other methods have found good agreement with wet chemical determinations (Mysen et al., 1985; Dingwell, 1991; Wilke et al., 2006). Dyar et al. (1987) found good agreement for a basalt and an andesite, but significant discrepancies for a rhyolite, although the overall uncertainties (±6%) in their study are comparatively high. Also, some studies have found good agreement between room temperature and cryogenic Mössbauer analyses of glasses (Helgason et al., 1989; Jayasuriya et al., 2004). As recoilless fraction should be temperature-dependent (Chen and Yang, 2007), this implies recoilless fraction effects on Fe^{3+}/Fe^{2+} determinations at room temperature could be small.

In contrast to these encouraging results, several studies have found discrepancies in application of uncorrected room temperature Mössbauer spectra to $Fe^{3+}/\Sigma Fe$ determinations. Lange and Carmichael (1989) reexamined the analyses of Mysen et al. (1985) and concluded that they show systematic discrepancies for Fe-rich glasses. In fact, compared to wet chemical analyses, there is a systematic 6% bias to greater $Fe^{3+}/\Sigma Fe$ for all Mössbauer data

presented by Mysen et al. (1985) and Dingwell (1991). Similarly, Righter et al. (2013) pointed out that the data of Wilke et al. (2006) actually suggest systematically greater $Fe^{3+}/\Sigma Fe$ from Mössbauer spectroscopy than from wet chemical analyses. We note that the wet chemical analyses for $Fe^{3+}/\Sigma Fe$ in glasses do not always agree with other methods or with microbeam determinations, but discrepancies are thought to be owing chiefly to the effects of dissolution of microphenocrysts and are therefore applicable to natural, but not synthetic, glasses (Bézos and Humler, 2005; Cottrell and Kelley, 2011). Mysen and Dubinsky (2004) used a Lorentzian absorption line shape to fit their Mössbauer spectra and found an 8% difference between $Fe^{3+}/\Sigma Fe$ measured on a synthetic basalt at 298 and 150 K. Finally, Ottonello et al. (2001) performed a thermodynamic analysis of the Fe^{3+} and Fe^{2+} contents of a wide array of glasses as a function of bulk composition, temperature, and oxygen fugacity and found that those analyzed by Mössbauer spectroscopy had a 14% bias to greater $Fe^{3+}/\Sigma Fe$ compared to glasses determined by wet chemistry. Owing to these observations, uncertainty lingers as to the accuracy of Mössbauer determinations of $Fe^{3+}/\Sigma Fe$ in glasses.

Fe^{2+} and Fe^{3+} are predominantly paramagnetic in silicate glasses, but Mössbauer spectra of some glasses also indicate a non-paramagnetic Fe component (Jayasuriya et al., 2004; O'Neill et al., 2006; Borisov and McCammon, 2010). In some cases, non-paramagnetic features are evident as well-resolved sextets, indicating either the presence of minor ferromagnetic precipitates or unrelaxed ferromagnetic interactions between Fe^{3+} ions in the

glass and incident γ rays. In other materials, the non-paramagnetic features are expressed only as a broadened absorption, and these occur owing to a super-paramagnetic phase with intermediate interactions (Borisov and McCammon, 2010). If these non-paramagnetic components are neglected or are too small to be quantified accurately from the Mössbauer spectra, the derived $Fe^{3+}/\Sigma Fe$ ratio may not be accurate.

To further investigate the accuracy of Mössbauer analyses of $Fe^{3+}/\Sigma Fe$ in silicate glasses, we conducted detailed low temperature Mössbauer investigations of andesitic glass. These allow us to determine directly the recoilless free fractions of Fe ions. To span glasses produced under different experimental conditions, we investigated a glass quenched from 1 atmosphere and one quenched from a high pressure device. For the low pressure glass, we also compared the results of our analysis to wet chemical determinations. Finally, because our initial results raised some questions about the structure of Fe ions in the quenched material, we also conducted magnetic susceptibility measurements to characterize non-magnetic components potentially present.

2 The Mössbauer Recoilless Fraction

The intensity or resonant absorption area of a particular component in a Mössbauer spectrum is determined by its recoilless fraction (f_T), which is the probability that a γ quantum will be absorbed resonantly. From both classical and quantum mechanical theories, $f(T)$ is given by

133 $$f(T) = e^{-k^2\langle x^2\rangle} \qquad (2)$$

134 where $\langle x^2 \rangle$ is the temperature-dependent mean-square atomic displacement, and k is the
135 wavenumber of the γ quantum (Chen and Yang, 2007). For a harmonic solid, the Debye
136 model for the vibrational modes of the lattice (Schroeder, 2000), $\langle x^2 \rangle$, $f(T)$ can be expressed
137 as

138 $$f(T) = \exp\left\{-\frac{3E_R}{2k_B\theta_D}\left[1+4\left(\frac{T}{\theta_D}\right)^2\int_0^{\theta_D/T}\frac{x}{e^x-1}dx\right]\right\}, \qquad (3)$$

139 where θ_D is the Debye temperature, k_B is the Boltzmann constant, E_R is the recoil energy,
140 which in turn is given by $E_R = E_\gamma/2Mc^2$, in which E_γ is the energy of the gamma rays (14.412
141 keV to excite ^{57}Fe), M is the mass of the absorber (^{57}Fe=56.935 amu), and c the velocity of
142 light (c=299792458 m/s).

143 A popular method to quantify recoilless fractions is to calculate them via Eqn. 3 using
144 Debye temperatures derived from the change of the Mössbauer center shift (CS) with
145 temperature (Niemantsverdriet et al., 1984b; De Grave et al., 1985; Dyar et al., 2012). The
146 center shift (CS), which is the location of the centroid of Mössbauer peaks in velocity relative
147 to a standard (α-iron in our case), has two components (Eqn. 4), the isomer shift (δ_{IS}), and the
148 second order Doppler shift (δ_{SOD}) (Niemantsverdriet et al., 1984b),

149 $$CS(T) = \delta_{IS} + \delta_{SOD}(T) \qquad (4)$$

150 The isomer shift is determined by the difference of s-electron density at the nucleus between
151 the source and the absorber, and is temperature independent, while the second-order Doppler

shift is dependent of the mean-square atomic velocity difference between the source and the absorber. Because the source is kept at room temperature, δ_{SOD} varies significantly with absorber temperature and can be parameterized with a Debye model (Pound and Rebka Jr, 1960),

$$CS(T) = \delta_{IS} - \frac{9k_B T}{2Mc}\left(\frac{T}{\theta_D}\right)^3 \int_0^{\theta_D/T}\left(1+\frac{x^3}{e^x-1}\right)dx \qquad (5)$$

The values of δ_{IS} and θ_D can be obtained from the CS of spectra measured over a range of temperatures using Eqn. 5, and then the recoilless fraction calculated from θ_D using Eqn. 3.

This center-shift method (CSM) for estimating recoilless fractions has been applied to Fe^{2+} and Fe^{3+} in a wide range of minerals (De Grave and Van Alboom, 1991) and most recently has been employed for detailed evaluation of $Fe^{3+}/\Sigma Fe$ in garnet (Dyar et al., 2012) and Fe^{2+} site occupancies in pyroxenes (Dyar et al., 2013). However, it may not be as accurate when applied to glasses, as the Debye model assumes harmonic behavior and therefore does not account for anharmonic contributions to atomic displacements, which are generally greater for amorphous materials (Kieffer, 1979). Studies comparing θ_D of glasses inferred from CS variations to θ_D determined directly from recoilless fractions deduced by other means have yielded mixed results. Komatsu and Soga (1980) found good agreement for a Na_2O-FeO-NiO-SiO_2 glass, but Oohata et al. (1994) found significant discrepancies for glassy V_2O_5-Fe_2O_3-P_2O_5. Thus, at least for glasses the center-shift method should be approached with caution.

A more direct method to quantify the recoilless fractions (f) is the relative method (RM) (Chen and Yang, 2007). For a thin sample in which the sample geometry does not change, the observed peak absorption area (AA) for each absorption are proportional to the concentration of the absorbing ion, N,

$$AA_T = f_T \mathrm{N} \qquad (6)$$

Consequently, so long as a phase transition or change in magnetic state is not traversed, the change in absorption area with temperature is only owing to the change in recoil-free fraction. If peak areas are normalized to that observed at a particular fixed temperature (T_0), $AA(T)/AA(T_0)$, which is equal to $f(T)/f(T_0)$, the ratio of recoilless-free fractions, depends only on the Debye temperature based on Eqn. (7)

$$\frac{AA(T)}{AA(T_0)} = \frac{f(T)}{f(T_0)} = \exp\left\{-\frac{6E_R}{k_B\theta_D}\left[\left(\frac{T}{\theta_D}\right)^2 \int_0^{\theta_D/T} \frac{x}{e^x-1}dx - \left(\frac{T_0}{\theta_D}\right)^2 \int_0^{\theta_D/T_0} \frac{x}{e^x-1}dx\right]\right\} \qquad (7)$$

Fitting the Debye temperature to values of $A(T)/A(T_0)$ from data collected over a range of temperatures allows calculations of the recoilless fraction at any temperature via Eqn. 3. Technically, application of this method to anharmonic solids is subject to the same uncertainty as the center shift method described above. However, so long as the measurements of $A(T)/A(T_0)$ span a significant fraction of the temperatures between 0 K and the temperature of interest (in this case, room temperature), the effect of anharmonicity on calculated absolute values of $f(T)$ will be small, as interpolation of the harmonic approximation (Eqn. 7) will empirically capture any anharmonic effects expressed over the

range of temperatures for which data are available .

3 Methods

3.1 Sample synthesis

Two different andesitic glasses were analyzed, both with essentially the same major element composition (Table 1), similar to that used by O'Neill et al. (2006), but quenched from different conditions. One, M544, was quenched at 3.5 GPa, 1600 °C as part of the high pressure study of Zhang and Hirschmann (in prep.), whereas the second, VF3, was quenched at 1 atm, 1400 °C and was produced expressly for this study.

The starting materials were prepared from reagent oxides (SiO_2, Al_2O_3, Fe_2O_3, TiO_2, MgO, FeO), silicates ($CaSiO_3$, Na_2SiO_3) and stoichiometric glasses (sanidine). For M544, all iron was added as Fe_2O_3 and 30% of the Fe_2O_3 consisted of $^{57}Fe_2O_3$ (Isoflex, Inc), with the balance derived from normal reagent oxide. For VF3, similar proportions of isotopically normal FeO and Fe_2O_3 were added. Prior to weighing, the SiO_2, Al_2O_3, TiO_2, and MgO were devolatilized by heating in a furnace at 1000 °C overnight. These reagants were then weighed and mixed with the silicates and sanidine by grinding in an agate mortar under ethanol at least one hour and then devolatilized a second time by annealing at 1000 °C for 48 hrs. Finally, the Fe_2O_3, previously at 800 °C for 1 hour and for VF3, with weighed FeO were added to the silicate mix by grinding under ethanol.

For the high pressure experiment, the starting material was loaded in a 2 mm diameter Pt capsule together with a mixture of Ru and RuO_2 which produces an oxygen fugacity similar to that of the magnetite/hematite buffer (O'Neill and Nell, 1997). Under these conditions, loss of Fe to the Pt capsule is negligible and dissolution of RuO_2 in the silicate melt is limited to <100 ppm (O'Neill et al., 2006). Further details of the capsule design are described in O'Neill et al. (2006) and Zhang and Hirschmann (in prep.). The experiment was performed at 3.5 GPa and 1600 °C for 4hrs in a 1000-ton Walker-style multi-anvil device with an 18/12 (octahedral edge length/WC truncation edge length) assembly (Dasgupta et al., 2004). Temperature was controlled with a Type D ($W_{97}Re_3/W_{75}Re_{25}$) thermocouple that was positioned immediately above the capsule and oriented axially with respect to the heater. Pressure uncertainties are believed to be ±0.3 GPa, and temperature uncertainties are believed to be ±10 °C (Dasgupta et al., 2004).

The VF3 glass was fused at 1400 °C for 24 hrs in a Deltech VT28 vertical gas mixing furnace in a Pt crucible with oxygen fugacity controlled using a mixture of O_2 and Ar and temperature monitored with a Type S ($Pt_{90}Rh_{10}/Pt_{100}$) thermocouple. Temperature uncertainties are believed to be ±5 °C based on a thermocouple calibration which yielded 1059 °C for melting of Au, which compares to 1064 °C value given by ITS90. The VF3 glass was quenched in a few seconds by being dropped into water. Electron microprobe analysis of

a section spanning the furthest and closest positions relative to the Pt hanging wire indicated that the major element concentrations of the glass are homogeneous.

3.2 Analytical Methods

3.2.1 Electron microprobe

Textures of the quenched glasses were examined by back-scattered electron (BSE) and secondary electron imaging (SEI) using the JEOL JXA-8900R electron microprobe (EPMA) at the University of Minnesota. Major element concentrations were quantified by wave-length-dispersive analysis using a 15kV acceleration voltage, 20 nA beam current and a beam focused to 5 μm diameter. Peak and background counting times were 15 s for standard analyses and 30 s for unknown samples. Data were acquired using the following diffractometer crystals: LiF for Ti kα, LiFH for Mn kα, Fe kα, PETJ for K kα, Ca kα, and TAP for Al kα, Mg kα, Si kα, and Na kα. Mineral and glass standards from (Jarosewich et al., 1980) were used, including basaltic glass for Mg kα, Ca kα, ilmenite for Ti kα, albite for Si kα, Al kα, Na kα, Mn-olivine for Fe kα, Mn kα, and microcline for K kα, and matrix corrections were computed with Probe for Windows software.

Besides VF3 and M544, MPI-DING glass ATHO-G (Jochum et al., 2006) and USGS glasses BCR-2G and BIR-1G (Jochum et al., 2005) were analyzed several glasses as secondary standards. Each of these was analyzed before VF3, between VF3 and M544 and after M544. The intensity data of standards and unknown samples, including secondary

245 standards were checked for time dependent intensity (TDI) changes. Si kα and Na kα using a
246 self-calibrated TDI correction and detected no TDI effect on other elements. Corrections
247 were also applied for minor Si and Al drift that occurred during the analysis period.

248 3.2.2 Mössbauer spectroscopy

249 Mössbauer spectroscopy was conducted with a constant acceleration spectrometer (Web
250 Research (currently SeeCo)) equipped with a Janis Nitrogen shielded Helium dewar at the
251 Institute for Rock Magnetism, University of Minnesota. A ^{57}Co/Rh source and Reuter Stokes
252 proportional Ar gas counter was employed. Data were collected over 512 channels, which
253 were then folded to produce 256 unique channels. Calibration was relative to a pure α-Fe foil
254 for which data were collected at room temperature (293 K). As M544 includes ~3% $^{57}Fe_2O_3$,
255 the M544 glass was crushed into fine powder with ethanol then diluted with powdered sugar,
256 while VF3 was analyzed as a pure powdered glass. The ^{57}Fe in both samples' was evenly
257 distributed in an approximately circular mount 12.7 mm in diameter, confined by Kapton tape.

258 To verify the precision of the center shifts and peak areas determined at the conditions of
259 data acquisition (collection times) at low temperature conditions, additional Mössbauer
260 spectra were collected for sample VF3 at room temperature for durations ranging from 1 to
261 72 hours both at with 6 mm/s and 12 mm/s velocity scales. As shown in Figs. S1 and S2, both
262 the Center Shift (CS) of Fe^{3+} and Fe^{2+}, and the $Fe^{3+}/\Sigma Fe$ determined from peak area ratios,
263 are consistent between 6 mm/s and 12mm/s scale and almost same when background counts

264 exceed ~0.3 X 10^6, irrespective of velocity scales, all parameters are listed in Table S1. All
265 other spectra were collected over at least one day and sufficient counts (>550000 cts/channel
266 for M544 and >220000 cts/channel for VF3) were accumulated to get reasonable statistical
267 error. Mössbauer thicknesses for M544 and VF3 were estimated to be ~1.91 and ~4.08
268 mg/cm^2 Fe, respectively, using the RECOIL algorithm (Rancourt et al., 1993) and assuming a
269 recoilless free fraction equal to unity.
270 The spectra were collected from 47 K to room temperature (298 K). A silicon diode was
271 used as cryogenic temperature sensor. A 50 Watt constant-current-source heater, controlled
272 by a Neocera LTC-21 temperature controller was used to adjust the sample temperature. All
273 Mössbauer spectra were fitted with the RECOIL software package (Lagarec and Rancourt,
274 1997).
275 3.2.3 Wet Chemistry
276 The FeO* content of VF3 was determined using the micro-colorimetric procedure,
277 improved by Wilson (1960). Analyses were carried out blind at the University of Michigan.
278 USGS standards QL and W-2a powdered rock standards (Govindaraju, 1994) were analyzed
279 as part of the same procedure.
280 3.2.4 Magnetization Measurements
281 Magnetic hysteresis loops determining the relationship between applied magnetic field
282 and sample magnetization (Tauxe, 1998) were determined at room temperature (293 K) using

a Princeton Measurements Corp. vibrating sample magnetometer in the Institute for Rock Magnetism, University of Minnesota, with maximum field of 1.5 T. Sample VF3, was analyzed as a powdered glass and M544 as a powdered glass mixed with powdered sugar. Hysteresis parameters were calculated using software developed at the Institute for Rock Magnetism and described fully in (Jackson and Solheid, 2010).

4 Results

4.1 Wet Chemical and EMPA determinations.

Electron microprobe analyses of the glasses and secondary standards established FeO*. Analyses reproduced the accepted FeO* concentrations of the standards almost perfectly with the largest discrepancy being 0.03 wt.% (Table 1), and so the resulting FeO* of the unknown glasses (VF3 9.29±0.22 wt.%; M544 8.92±0.12 wt.%; 2σ) are believed to have high accuracy.

Wet chemical analysis of VF3 glass was repeated 4 times, resulting in FeO of 2.99±0.12 wt%, (2σ). Analyses of USGS standards, QL and W-2a, performed at the same time resulted in FeO contents that were systematically lower than accepted values (Govindaraju, 1994) by 4%, and so the results of VF3 have been adjusted accordingly, to 3.10±0.24 wt%, (2σ) (Table 2). We believe that the systematic discrepancy may be owing to the finely powdered standards, which were ground to grain sizes similar to the unknowns. The fine powdering results in some retention of starting material in the holding beaker. Combining the FeO* from

EMPA with FeO from wet chemistry, the resulting $Fe^{3+}/\Sigma Fe$ in VF3 is 0.666±0.030 (2σ) (Table 2).

4.2 Mössbauer Spectroscopy

Mössbauer spectra of VF3 and M544 have broadened line-shapes typical of silicate glasses and can be well-accommodated by distribution fitting methods (Alberto et al., 1996; Rossano et al., 1999; O'Neill et al., 2006; Rossano et al., 2008; Borisov and McCammon, 2010). Spectra consist chiefly of two quadrupole doublets, one originating from paramagnetic ferric and the other from ferrous iron. There is no obvious evidence of sextets in the spectra with velocity scale up to 12 mm/s. Such sextets are commonly present in quenched mafic glasses (Jayasuriya et al., 2004; O'Neill et al., 2006; Borisov and McCammon, 2010) and are indicative of a ferromagnetic component. Thus, the Fe in the glasses is dominantly paramagnetic Fe^{2+} and Fe^{3+}. The Fe thicknesses estimated for M544 and VF3 are expected to have negligible effect on determined Mössbauer parameters, and this was verified by comparing uncorrected spectra with those corrected using the pre-analysis thickness calculation available in the RECOIL package.

Preliminary fitting of the Mössbauer data was performed by treating the spectra solely as the result of two paramagnetic doublets by assuming that the Lorentzian half widths at half maximum (L HWHM) for all sub-spectra are the same (Lagarec and Rancourt, 1997). Each doublet was fit with as a two dimensional (2D) distribution, whose parameters consist of the

center shift (CS), the quadrupole splitting (QS), and their respective Gaussian widths, δ_{CS} and δ_{QS}, We did not consider the correlation between CS and QS for Fe^{3+}, (θ), or the correlation between the CS distribution and the QS distribution of QS, because the analysis of Alberto et al. (1996) showed that these should be effectively negligible for Fe^{3+} in silicate glasses in low concentrations (5~15 wt.% Fe_2O_3), (θ). The fit of the Fe^{2+} paramagnetic component considers these correlations. All the hyperfine parameters and their uncertainties were calculated based on a bootstrap method and are cataloged in Table S2. The quality of these fits is characterized by reduced chi squared (χ^2) values, which are also listed in Table S2 and demonstrates that the fitting is robust.

From the Mössbauer spectra collected at room temperature (Fig. 1a and Fig. 1c), for Fe^{3+} in M544, CS = 0.334 mm/s and QS = 1.166 mm/s, and for Fe^{3+} in VF3, CS = 0.283 mm/s and QS = 1.148 mm/s, whilst for Fe^{2+} in M544, CS = 1.080 mm/s and QS = 2.013 mm/s, for Fe^{2+} in VF3, CS = 0.994 mm/s and QS = 1.754 mm/s. These parameters are similar to those previously reported for silicate glasses (Alberto et al., 1996; Jayasuriya et al., 2004; O'Neill et al., 2006; Borisov and McCammon, 2010). Proportions of $Fe^{3+}/\Sigma Fe$ in M544 and VF3, judged solely from the area ratios of the 293 K paramagnetic doublets are 0.6001±0.0083, 2σ, and 0.685±0.014, 2σ, respectively.

Low temperature Mössbauer spectra show features similar to those at room temperature, as illustrated at 67K for M544 and VF3 (Fig. 1b and 1d). With increasing temperature, the

relative area under the Fe^{2+} doublet diminishes compared to that of Fe^{3+} (Table S3), and the normalized area ratios decrease for both Fe^{3+} and Fe^{2+} (Fig. 2). As the $Fe^{3+}/(Fe^{2+}+Fe^{3+})$ ratio of the sample does not change, this temperature dependence is best understood as a change in the relative recoilless fractions for Fe^{3+} and Fe^{2+}, as expected from Eqn. 1. Also, center shifts (CS) increase with decreasing temperature, consistent with the contributions of the second order Doppler shift (Eqns. 4, 5) (Fig. 3). Each of these observations can be used to determine Mössbauer Debye temperatures and in turn can be used to model the relationship between temperature and recoilless fraction for these glasses.

Mössbauer Debye temperatures determined by direct measurement of the temperature dependent relative areas of the Mössbauer doublets (Eqn. 7) are calculated by normalizing to measurements at low temperature (47K). Least squares analysis of normalized peak areas gives Mössbauer Debye temperatures (θ_D) of 373±39 K and 305±30 K, in 2σ, for Fe^{3+} and Fe^{2+} respectively for M544 and 352±30 K and 269±27 K, in 2σ, respectively for VF3. Similarly, Mössbauer Debye temperatures and intrinsic isomer shifts, δ_{IS}, can be determined from a least squares fit to the CS versus temperature trends (Fig. 3) (Eqn. 5), yielding, for M544, δ_{IS}=0.576±0.026 mm/s and θ_D=506±114 K (Fe^{3+}) and δ_{IS}=1.314±0.016 mm/s and θ_D=295 ± 89 K (Fe^{2+}) and for VF3, δ_{IS}=0.524±0.016 mm/s and θ_D=466±78 K (Fe^{3+}) and δ_{IS}=1.233±0.017 mm/s and θ_D=235±114 K, all uncertainties are 2σ.

From these determinations of Mössbauer Debye temperatures and Eqn. 3, recoilless fractions can be calculated as a function of temperature (Table S3). At 293 K, the value of C in Eqn.1, calculated with θ_D derived from the relative method (C^{RM}) is 1.151±0.118 and 1.256±0.0153, for M544 and VF3 respectively. Values calculated at 293 K from CS data (C^{CSM}) are distinctly higher: C^{CSM}, is 1.305±0.146 for M544 and 1.762±1.188 for VF3 (Table S3). Resulting calculated values of $Fe^{3+}/\Sigma Fe$, based on these values and 293 K area ratios are, for M544, 0.569 (RM) and 0.532 (CSM) and, for VF3, 0.634 (RM) and 0.552 (CSM).

4.3 Magnetic hysteresis

Measurements of sample magnetization versus applied field (hysteresis loops) reveal hysteresis in both glasses, indicating a minor ferromagnetic component (Fig. 5) with superparamagnetic behavior in addition to a paramagnetic component. A purely paramagnetic material would produce a simple linear relationship between applied field and magnetic moment. A small ferromagnetic contribution would saturate in lower fields (0.3 Tesla for magnetite) and typically has magnetization intensities several orders of magnitude higher than a paramagnetic material in a 1.5 Tesla field. For glass M544, the sigmoidal shape of the magnetization curves shown in Fig. 5a, with saturation around 500 mT are indicative of superparamagnetic behavior, as is treated Fig 2.19c in Tauxe (1998). This contrasts with the observed Mössbauer spectrum (Fig. 1), which shows only simple paramagnetic doublets.

This seeming discrepancy is in large part owing to the admixture of sugar (which is diamagnetic) with glass in the M544 sample mount (Fig. S3).

For VF3, the raw data produces a nearly linear relationship between magnetization and applied field (Fig. 5b), indicating very little ferromagnetic contribution to the hysteresis loop (Dunlop and Özdemir, 2001). Yet, the small deviation from linearity, evident in the slope-corrected loop, shows that a minor superparamagnetic component is also present (Dunlop and Özdemir, 2001) This component is not clearly evident in the Mössbauer spectra (Fig. 1), presumably because it is small, but failure to account for its contribution may lead to overestimation or underestimation of the $Fe^{3+}/\Sigma Fe$ ratio determined from Mössbauer spectra, depending on the ratio of $Fe^{3+}/\Sigma Fe$ in this minor phase. Note that unrelaxed Fe^{3+} in the silicate glass cannot account for the magnetic hysteresis behavior of the sample, as the time constant of applied magnetic field is far greater than the relaxation time of isolated Fe^{3+} ions (Chen and Yang, 2007). Sample M544 has a stronger ferromagnetic signal, but again with near zero coercivity indicating a superparamagnetic phase.

Based on the measured saturation magnetizations (σ_s) (M544: 0.5235 Am^2/kg; VF3: 0.0426 Am^2/kg, Fig. 5), the fraction of nonparamagnetic nanophase present can be estimated provided that the identity and magnetic characteristics of the ferromagnetic nanophase are known. Although several possibilities exist, the most likely phase is a Fe-Mg ferrite (Fe_3O_4 - $MgFe_2O_4$) solid solution. For VF3, if we assume the ferromagnetic nanophase is pure Fe_3O_4,

for which the saturation magnetization, σ_s=92 Am^2/kg (Li et al., 2006), the resulting Fe in the ferromagnetic nanophase [$(Fe^{2+}+Fe^{3+})_{Fe3O4}/\Sigma Fe$] is 0.0043. If we assume it is pure $MgFe_2O_4$, whose σ_s=33.4 Am^2/kg (Šepelák et al., 2007), $Fe^{3+}_{MgFe2O4}/\Sigma Fe$ is 0.0118. Ferrite solid solutions will be intermediate between these bounds, and so the contribution of the non-paramagnetic material to $Fe^{3+}/\Sigma Fe$ of the bulk material is small but constrained.

5 Discussion

5.1 Estimating recoilless fractions from center shift versus relative methods

For both the VF3 and M544 glasses, estimates of ferric Debye temperatures are much greater from the CS method than from the relative method, while estimates of ferrous Debye temperatures from the two methods are similar, as also was observed in previous studies (Niemantsverdriet et al., 1984a; Oohata et al., 1994). These discrepancies are presumably owing to anharmonicity in the glasses, and the resulting inaccuracy of the Debye model. The differences in the two methods produce significant differences in recoilless fraction estimates of $Fe^{3+}/\Sigma Fe$ of the glasses (Fig. 4). We argue that the RM yields more accurate estimates for these glasses and that the CS method is in this case less reliable. First, as previously mentioned, the RM is based on the effect of temperature on the areas of the observed Mössbauer doublets (Fig. 2), and so the Debye model functions chiefly as an empirical method to interpolate measured changes in recoilless fraction as a function of temperature. Translation of the temperature dependence of the CS to recoilless fraction is more reliant on

the accuracy of the Debye theory. Second, because the $Fe^{3+}/\Sigma Fe$ of the silicate does not vary with temperature, an accurate recoilless fraction correction should produce a nearly constant ratio at all temperatures. Those determined using the CS method vary with temperature, whereas those from the RM method are more nearly temperature-independent (Fig. 4). Accurate values of recoilless fraction should produce the same calculated $Fe^{3+}/\Sigma Fe$ at all temperatures (Eqn.1), suggesting that the values of C_T calculated with the RM method are more accurate and that those calculated with the CS method overestimate recoilless effects on $Fe^{3+}/\Sigma Fe$ determinations for these andesitic glasses (Fig. 4).

5.2 Modeling nonparamagnetic effects on $Fe^{3+}/\Sigma Fe$ of the quenched glasses

Correction for recoilless effects on paramagnetic Mössbauer doublets does not address the influence of non-paramagnetic nanophases on the accuracy of room temperature Mössbauer determinations of $Fe^{3+}/\Sigma Fe$. Consequently, we refit the room temperature Mössbauer spectrum for VF3 by including superparamagnetic phase of fixed proportion based on the magnetic hysteresis loop analysis above (0.43% Fe_3O_4 or 1.18% $MgFe_2O_4$ for VF3, respectively). As superparamagnetic material will show six peaks at low temperature and collapse to one peak as temperature increases (Mørup et al., 1976; Mørup and Tronc, 1994). To investigate whether the superparamagnetic material observed in the hysteresis measurements adds uncertainty to $Fe^{3+}/\Sigma Fe$ ratios calculated from Mossbauer spectra, we included a superparamagnetic component to the fit paramagnetic spectrum, the extra phase is

433 expected to produce an extra single absorption peak in a magnetic site centered at CS=0
434 mm/s at room temperature. Because the xVBF method is applied, the Lorentzian half width at
435 half maximum (L HWHM) for all sub-spectra is the same (Lagarec and Rancourt, 1997) and
436 so no Gaussian width is required to fit this extra absorption peak. Resulting fits are shown in
437 Figs. 1e and 1f, and the detailed fitting parameters are given in Table S4. The resulting
438 $Fe^{3+}/\Sigma Fe$ ratios are essentially indistinguishable regardless of whether the nanophase is
439 assumed to be Fe_3O_4 or $MgFe_2O_4$. Specifically, the resulting $Fe^{3+}/\Sigma Fe$ ratios are 0.685 if the
440 ferrite is pure Fe_3O_4 and 0.684 if it is $MgFe_2O_4$. These are not distinguishable from one
441 another or from the ratio (0.685) derived by neglecting the nonparamagnetic component,
442 indicating that the influence of the non-paramagnetic component on $Fe^{3+}/\Sigma Fe$ on this glass is
443 small.

444 The $Fe^{3+}/\Sigma Fe$ ratios in the previous paragraph neglect the effects of recoilless fractions.
445 Although the overall effect of the non-paramagnetic phase is small, for thoroughness it is
446 appropriate to consider recoilless fractions not only for the paramagnetic doublets, as already
447 described, but also for the nanophase oxides. For Fe_3O_4, θ_D=334±10 K for Fe^{3+} and
448 θ_D=314±10 K for Fe^{2+} (Sawatzky et al., 1969), giving recoilless fractions at room
449 temperature (calculated from Eqn. 3) of $f(Fe^{3+})_{Fe3O4}$=0.693 and $f(Fe^{2+})_{Fe3O4}$=0.661. No similar
450 data are available for $MgFe_2O_4$, so we assume that θ_D for Fe^{3+} is the same as in Fe_3O_4. The

451 resulting calculated $Fe^{3+}/\Sigma Fe$ ratio for VF3 equals 0.633 or 0.632 respectively, assuming that
452 the nonparamagnetic phase is pure Fe_3O_4 or $MgFe_2O_4$.

453 ***5.3 Superparamagnetism in quenched glasses***

454 The magnetic hysteresis of the quenched glasses establish that a small fraction of the Fe is
455 present as a superparamagnetic phase, which suggests that nanometer-scale precipitates of
456 Fe-oxide were produced during quench of the silicate liquid. The formation of such
457 precipitates may have been promoted by the comparatively high Fe_2O_3 content (~6 wt%) of
458 the melt. There is little reason to believe that their formation affected the $Fe^{3+}/\Sigma Fe$ of the
459 aggregate quenched material, and so long as the nanophase is accounted for in the fitting of
460 the spectrum, it should not compromise the accuracy of the inferred $Fe^{3+}/\Sigma Fe$ of the silicate
461 liquid present prior to quench.

462 Superparamagnetic behavior has been documented in otherwise fresh natural basaltic
463 glasses (Pick and Tauxe, 1994), and in Fe-rich basaltic glasses quenched in the laboratory
464 (Bowles et al., 2011) but is not generally considered to contribute to Mössbauer spectra of
465 laboratory-quenched glasses. Non-paramagnetic components of Mössbauer spectra, including
466 broad absorptions approximately symmetric about CS=0 mm/s as well as sextets, are a
467 common feature in such glasses, in many cases comprising a larger fraction of the Fe than
468 documented for VF3 or M544 (Jayasuriya et al., 2004; O'Neill et al., 2006; Borisov and
469 McCammon, 2010; Weigel et al., 2010). These non-paramagnetic components are commonly

attributed to unrelaxed ferromagnetic behavior of Fe^{3+} ions in the glass, in part because of skepticism that superparamagnetic precipitates form from rapidly cooled glasses (Weigel et al., 2010). Documentation of nanophase oxides from rapidly cooled glasses in this study suggests that superparamagnetic components may be more common contributors to Mössbauer spectra of laboratory-quenched glasses than previously supposed, particularly in cases where a single symmetric peak is observed, but also in cases when non-paramagnetic features are not obvious from casual inspection of the Mössbauer results. Depending on the size and domain structure of the particles, such precipitates could also contribute to ferromagnetic sextets in Mössbauer spectra. This would be of particular concern, as such phases, presumably rich in Fe_3O_4, would contain both Fe^{2+} and Fe^{3+}, whereas normal attribution as unrelaxed ions considers them to consist solely as Fe^{3+}.

5.4 Wet chemical vs. Mössbauer determination of $Fe^{3+}/\Sigma Fe$

Returning to the controversy of the accuracy of $Fe^{3+}/\Sigma Fe$ ratio determined from Mössbauer spectra collected at room temperature (Mysen et al., 1985; Dyar et al., 1987; Helgason et al., 1989; Lange and Carmichael, 1989; Dingwell, 1991; Ottonello et al., 2001; Jayasuriya et al., 2004; Mysen and Dubinsky, 2004; Rossano et al., 2008; Righter et al., 2013), Fig. 6 compares combined wet chemical/microprobe determination of $Fe^{3+}/\Sigma Fe$ for andesitic glass VF3 with different treatments of the Mössbauer spectra. In general, distinctions in $Fe^{3+}/\Sigma Fe$ ratio determined from different treatments of the Mössbauer spectra

and wet chemistry are small and within 2σ analytical uncertainty envelopes. The $Fe^{3+}/\Sigma Fe$ ratio derived from temperature uncorrected for recoilless effects or for non-paramagnetic components agrees with that determined by wet chemistry with a relative difference about 3%. However, $Fe^{3+}/\Sigma Fe$ values corrected for recoilless fraction have a large uncertainties at 2σ. One possible reason for these uncertainties could be owing to insufficient constraints on the Debye temperatures, due to too few measurements made as a function of temperature (Fig. 2), or because of insufficient precision in peak locations and areas due to poor counting statistics. The latter may indicate that the error bands in $Fe^{3+}/\Sigma Fe$ propagated from the uncertainties in individual parameter determinations are exaggerated, as the stability of determined Mossbauer parameters as a function of counting time (Figs. S1 and S2) suggests that longer counting times results in smaller errors without appreciable changes in values of determined parameters. A more general factor that may apply beyond the details of data collection in this particular study is that Mössbauer spectra of glasses have comparatively broad peaks, making precise determinations of CSs and peak areas more challenging than for minerals. The former reasons indicate that high uncertainty in recoilless fractions, and therefore $Fe^{3+}/\Sigma Fe$ are specific to the conditions of this study, whereas the last reason highlights a more general challenge to application of Mössbauer spectroscopy to $Fe^{3+}/\Sigma Fe$ determinations in glass.

Implication

Room temperature Mössbauer spectroscopy yields accurate $Fe^{3+}/\Sigma Fe$ ratios in silicate glasses within normal analytical uncertainties, but with a small systematic bias to higher values compared to wet chemical or recoilless fraction-corrected determinations. A common method for estimating recoilless fractions by measurement of the temperature dependence of the Mössbauer center-shift may not be accurate for glasses, but relative peak height methods appear to be more robust. Nanophase magnetic precipitates can form in rapidly quenched glasses and, if not accounted for properly, can bias Mössbauer-determined $Fe^{3+}/\Sigma Fe$ ratios. Therefore, accurate determination of $Fe^{3+}/\Sigma Fe$ ratios in silicate glasses by Mössbauer spectroscopy requires consideration of the recoilless fraction.

Acknowledgments

We are grateful for conversations with B. Moskowitz regarding the magnetic features of the glasses. We are also grateful to Tony Withers and Jed Mosenfelder for assistance and support in the experimental petrology laboratory. This work supported by the NASA Cosmochemistry program grant NNX11AG64G. And this is publication 1503 of the Institute for Rock Magnetism, which is supported by grants from the Instruments and Facilities Program, Division of Earth Science, National Science Foundation.

Reference

Alberto, H.V., Pinto da Cunha, J.L., Mysen, B.O., Gil, J.M., and Ayres de Campos, N. (1996) Analysis of Mössbauer spectra of silicate glasses using a two-dimensional Gaussian distribution of hyperfine parameters. Journal of Non-Crystalline Solids, 194(1-2), 48-57.

528 Bancroft, M.G., and Brown, J.R. (1975) A Mössbauer study of coexisting hornblendes and biotites:
529 quantitative Fe^{3+}/Fe^{2+} ratios. American Mineralogist, 60, 265-272.
530 Berry, A.J., Danyushevsky, L.V., O'Neill, H.S.C., Newville, M., and Sutton, S.R. (2008) Oxidation
531 state of iron in komatiitic melt inclusions indicates hot Archaean mantle. Nature, 455(7215),
532 960-963.
533 Bézos, A., and Humler, E. (2005) The $Fe^{3+}/\Sigma Fe$ ratios of MORB glasses and their implications for
534 mantle melting. Geochimica et Cosmochimica Acta, 69(3), 711-725.
535 Borisov, A., and McCammon, C. (2010) The effect of silica on ferric/ferrous ratio in silicate melts:
536 An experimental study using Mössbauer spectroscopy. American Mineralogist, 95(4), 545-
537 555.
538 Bowles, J.A., Gee, J.S., Burgess, K., and Cooper, R.F. (2011) Timing of magnetite formation in
539 basaltic glass: Insights from synthetic analogs and relevance for geomagnetic paleointensity
540 analyses. Geochemistry, Geophysics, Geosystems, 12(2).
541 Carmichael, I.S.E., and Kress, V.C. (1988) Stoichiometry of the iron oxidation reaction in silicate
542 melts. American Mineralogist, 73(11-12), 1267-1274.
543 Carmichael, I.S.E., and Kress, V.C. (1991) The compressibility of silicate liquids containing Fe_2O_3
544 and the effect of composition, temperature, oxygen fugacity and pressure on their redox states.
545 Contributions to Mineralogy and Petrology, 108, 82-92.
546 Chen, Y.-L., and Yang, D.-P. (2007) Mössbauer effect in lattice dynamics: experimental techniques
547 and applications. John Wiley & Sons.
548 Christie, D.M., Carmichael, I.S.E., and Langmuir, C.H. (1986) Oxidation states of mid-ocean ridge
549 basalt glasses. Earth and Planetary Science Letters, 79(3-4), 397-411.
550 Cottrell, E., and Kelley, K.A. (2011) The oxidation state of Fe in MORB glasses and the oxygen
551 fugacity of the upper mantle. Earth and Planetary Science Letters, 305, 270-282.
552 -. (2013) Redox heterogeneity in mid-ocean ridge basalts as a function of mantle source. Science,
553 340(6138), 1314-1317.
554 Cottrell, E., Kelley, K.A., Lanzirotti, A., and Fischer, R.A. (2009) High-precision determination of
555 iron oxidation state in silicate glasses using XANES. Chemical Geology, 268, 167-179.
556 Dasgupta, R., Hirschmann, M.M., and Withers, A.C. (2004) Deep global cycling of carbon
557 constrained by the solidus of anhydrous, carbonated eclogite under upper mantle conditions.
558 Earth and Planetary Science Letters, 227(1-2), 73-85.
559 De Grave, E., and Van Alboom, A. (1991) Evaluation of ferrous and ferric Mössbauer fractions.
560 Physics and Chemistry of Minerals, 18, 337-342.
561 De Grave, E., Verbeeck, A.E., and Chambaere, D.G. (1985) Influence of small aluminum
562 substitutions on the hematite lattice. Physics Letters A, 107(4), 181-184.
563 Dingwell, D.B. (1991) Redox viscometry of some Fe-bearing silicate melts. American Mineralogist,
564 76, 1560-1562.

565 Dunlop, D.J., and Özdemir, Ö. (2001) Rock Magnetism: Fundamentals and Frontiers. Cambridge
566 University Press.
567 Dyar, M.D., Breves, E.A., Emerson, E., Bell, S.W., Nelms, M., Ozanne, M.V., Peel, S.E., Carmosino,
568 M.L., Tucker, J.M., Gunter, M.E., Delaney, J.S., Lanzirotti, A., and Woodland, A.B. (2012)
569 Accurate determination of ferric iron in garnets by bulk Mössbauer spectroscopy and
570 synchrotron micro-XANES. American Mineralogist, 97(10), 1726-1740.
571 Dyar, M.D., Klima, R.L., Fleagle, A., and Peel, S.E. (2013) Fundamental Mössbauer parameters of
572 synthetic Ca-Mg-Fe pyroxenes. American Mineralogist, 98(7), 1172-1186.
573 Dyar, M.D., Naney, M.T., and Swanson, S.E. (1987) Effects of quench methods on Fe^{3+}/Fe^{2+} ratios: A
574 Mössbauer and wet-chemical study. American Mineralogist, 72, 792-800.
575 Govindaraju, K. (1994) 1994 compilation of working values and sample description for 383
576 geostandards. Geostandards newsletter, 18(S1), 1-158.
577 Helgason, Ö., Steinthorsson, S., and Mørup, S. (1989) The ferric/ferrous ratio in basalt melts at
578 different oxygen pressures. Hyperfine Interactions, 45(1-4), 287-294.
579 Jackson, M., and Solheid, P. (2010) On the quantitative analysis and evaluation of magnetic hysteresis
580 data. Geochemistry, Geophysics, Geosystems, 11(4).
581 Jarosewich, E., Nelen, J.A., and Norberg, J.A. (1980) Reference Samples for Electron Microprobe
582 Analysis*. Geostandards Newsletter, 4(1), 43-47.
583 Jayasuriya, K.D., O'Neill, H.S.C., Berry, A.J., and Campbell, S.J. (2004) A Mössbauer study of the
584 oxidation state of Fe in silicate melts. American Mineralogist, 89, 1597-1609.
585 Jochum, K.P., Stoll, B., Herwig, K., Willbold, M., Hofmann, A.W., Amini, M., Aarburg, S.,
586 Abouchami, W., Hellebrand, E., Mocek, B., Raczek, I., Stracke, A., Alard, O., Bouman, C.,
587 Becker, S., Dücking, M., Brätz, H., Klemd, R., de Bruin, D., Canil, D., Cornell, D., de Hoog,
588 C.-J., Dalpé, C., Danyushevsky, L., Eisenhauer, A., Gao, Y., Snow, J.E., Groschopf, N.,
589 Günther, D., Latkoczy, C., Guillong, M., Hauri, E.H., Höfer, H.E., Lahaye, Y., Horz, K.,
590 Jacob, D.E., Kasemann, S.A., Kent, A.J.R., Ludwig, T., Zack, T., Mason, P.R.D., Meixner, A.,
591 Rosner, M., Misawa, K., Nash, B.P., Pfänder, J., Premo, W.R., Sun, W.D., Tiepolo, M.,
592 Vannucci, R., Vennemann, T., Wayne, D., and Woodhead, J.D. (2006) MPI-DING reference
593 glasses for in situ microanalysis: New reference values for element concentrations and isotope
594 ratios. Geochemistry, Geophysics, Geosystems, 7(2).
595 Jochum, K.P., Willbold, M., Raczek, I., Stoll, B., and Herwig, K. (2005) Chemical characterisation of
596 the USGS reference glasses GSA-1G, GSC-1G, GSD-1G, GSE-1G, BCR-2G, BHVO-2G and
597 BIR-1G using EPMA, ID-TIMS, ID-ICP-MS and LA-ICP-MS. Geostandards and
598 Geoanalytical Research, 29(3), 285-302.
599 Kelley, K.A., and Cottrell, E. (2009) Water and the oxidation state of subduction zone magmas.
600 Science, 325(5940), 605-607.

Kieffer, S.W. (1979) Thermodynamics and lattice vibrations of minerals: 3. Lattice dynamics and an approximation for minerals with application to simple substances and framework silicates. Reviews of Geophysics, 17(1), 35-59.

Komatsu, T., and Soga, N. (1980) ESR and Mo□ssbauer studies of crystallization process of sodium iron silicate glass. The Journal of Chemical Physics, 72(3), 1781-1785.

Lagarec, K., and Rancourt, D.G. (1997) Extended Voigt-based analytic lineshape method for determining N-dimensional correlated hyperfine parameter distributions in Mössbauer spectroscopy. Nuclear Instruments and Methods in Physics Research Section B: Beam Interactions with Materials and Atoms, 129(2), 266-280.

Lange, R.A., and Carmichael, I.S.E. (1989) Ferric-ferrous equilibria in Na_2O-FeO-Fe_2O_3-SiO_2 melts - effects of analytical techniques on derived partial molar volumes. Geochimica et Cosmochimica Acta, 53(9), 2195-2204.

Li, B., Jia, D., Zhou, Y., Hu, Q., and Cai, W. (2006) In situ hybridization to chitosan/magnetite nanocomposite induced by the magnetic field. Journal of Magnetism and Magnetic Materials, 306(2), 223-227.

McCammon, C.C., and Kopylova, M.G. (2004) A redox profile of the slave mantle and oxygen fugacity control in the cratonic mantle. Contributions to Mineralogy and Petrology, 148(1), 55-68.

Mørup, S., Topsøe, H., and Lipka, J. (1976) Modified theory for Mössbauer spectra of superparamagnetic particles: application to Fe_3O_4. Le Journal de Physique Colloques, 37(C6), C6-287-C6-290.

Mørup, S., and Tronc, E. (1994) Superparamagnetic relaxation of weakly interacting particles. Physical review letters, 72(20), 3278.

Mysen, B.O., Carmichael, I.S.E., and Virgo, D. (1985) A comparison of iron redox ratios in silicate glasses determined by wet-chemical and ^{57}Fe Mössbauer resonant absorption methods. Contributions to Mineralogy and Petrology, 90(2-3), 101-106.

Mysen, B.O., and Dubinsky, E.V. (2004) Melt structural control on olivine/melt element partitioning of Ca and Mn. Geochimica et Cosmochimica Acta, 68(7), 1617-1633.

Mysen, B.O., and Virgo, D. (1985) Iron-bearing silicate melts: relations between pressure and redox equilibria. Physics and Chemistry of Minerals, 12(4), 191-200.

-. (1986) Volatiles in silicate melts at high pressure and temperature: 1. Interaction between OH groups and Si^{4+}, Al^{3+}, Ca^{2+}, Na^{+} and H^{+}. Chemical Geology, 57, 303-331.

Niemantsverdriet, J.W., Flipse, C.F.J., Selman, B., Van Loef, J.J., and Van Der Kraan, A.M. (1984a) Influence of particle motion on the Mössbauer effect in microcrystals α-FeOOH and α-Fe_2O_3. Physics Letters A, 100(8), 445-447.

Niemantsverdriet, J.W., Van der Kraan, A.M., and Delgass, W.N. (1984b) Characterization of surface phases in bimetallic $FeRhSiO_2$ catalysts by in situ Mössbauer spectroscopy at cryogenic temperatures. Journal of Catalysis, 89(1), 138-149.

O'Neill, H.S.C., Berry, A.J., McCammon, C., Jayasuriya, K.D., Campbell, S.J., and Foran, G. (2006) An experimental determination of the effect of pressure on the $Fe^{3+}/\Sigma Fe$ ratio of an anhydrous silicate melt to 3.0 GPa. American Mineralogist, 91(2-3), 404-412.

O'Neill, H.S.C., and Nell, J. (1997) Gibbs free energies of formation of RuO_2, IrO_2, and OsO_2: A high-temperature electrochemical and calorimetric study. Geochimica Et Cosmochimica Acta, 61(24), 5279-5293.

Oohata, T., Shirahata, K., Toriyama, T., Inamura, T., Yoshino, K., and Iijima, H. (1994) Mössbauer spectroscopy of a semiconductive phosphate glass ($10V_2O_5$-$30Fe_2O_3$-$60P_2O_5$) at low temperature. Hyperfine Interactions, 94(1), 2131-2136.

Ottonello, G., Moretti, R., Marini, L., and Zuccolini, M.V. (2001) Oxidation state of iron in silicate glasses and melts: a thermochemical model. Chemical Geology, 174, 157-179.

Pick, T., and Tauxe, L. (1994) Characteristics of magnetite in submarine basaltic glass. Geophysical Journal International, 119(1), 116-128.

Pound, R.V., and Rebka Jr, G.A. (1960) Variation with temperature of the energy of recoil-free gamma rays from solids. Physical Review Letters, 4(6), 274.

Rancourt, D.G., McDonald, A.M., Lalonde, A.E., and Ping, J.Y. (1993) Mössbauer absorber thicknesses for accurate site populations in Fe-bearing minerals. American Mineralogist, 78(1-2), 1-7.

Righter, K., Danielson, L.R., Pando, K., Morris, R.V., Graff, T.G., Agresti, D.G., Martin, A.M., Sutton, S.R., Newville, M., and Lanzirotti, A. (2013) Redox systematics of martian magmas with implications for magnetite stability. American Mineralogist, 98(4), 616-628

Rossano, S., Balan, E., Morin, G., Bauer, J.P., Calas, G., and Brouder, C. (1999) Fe Mössbauer spectroscopy of tektites. Physics and Chemistry of Minerals, 26, 530-538.

Rossano, S., Behrens, H., and Wilke, M. (2008) Advanced analyses of ^{57}Fe Mössbauer data of alumino-silicate glasses. Physics and Chemistry of Minerals, 35, 77-93.

Sack, R.O., Carmichael, I.S.E., Rivers, M., and Ghiorso, M.S. (1981) Ferric-ferrous equilibria in natural silicate liquids at 1 bar. Contributions to Mineralogy and Petrology, 75(4), 369-376.

Sawatzky, G.A., Van Der Woude, F., and Morrish, A.H. (1969) Mössbauer study of several ferrimagnetic spinels. Physical Review, 187(2), 747-757.

Schroeder, D.V. (2000) An Introduction to Thermal Physics. Addison-Wesley.

Šepelák, V., Bergmann, I., Menzel, D., Feldhoff, A., Heitjans, P., Litterst, F.J., and Becker, K.D. (2007) Magnetization enhancement in nanosized $MgFe_2O_4$ prepared by mechanosynthesis. Journal of Magnetism and Magnetic Materials, 316(2), 764-767.

Tauxe, L. (1998) Paleomagnetic Principles and practice. Kluwer Academic Publishers.

Weigel, C., McCammon, C., and Keppler, H. (2010) High-temperature Mössbauer spectroscopy: A probe for the relaxation time of Fe species in silicate melts and glasses. American Mineralogist, 95(11-12), 1701-1707.

Wilke, M., Farges, F., Petit, P.-E., Gordon E Brown, Jr., and Martin, F. (2001) Oxidation state and coordination of Fe in minerals: An Fe K-XANES spectroscopic study. American Mineralogist, 86(5-6), 714-730.

Wilke, M., Schmidt, C., Farges, F., Malavergne, V., Gautron, L., Simionovici, A., Hahn, M., and Petit, P.-E. (2006) Structural environment of iron in hydrous aluminosilicate glass and melt-evidence from X-ray absorption spectroscopy. Chemical Geology, 229(1-3), 144-161.

Wilson, A.D. (1960) The micro-determination of ferrous iron in silicate minerals by a volumetric and a colorimetric method. The Analyst, 85(1016), 823-827.

Woodland, A.B., and Ross II, C.R. (1994) A crystallographic and Mössbauer spectroscopy study of $Fe_3^{2+}Al_2Si_3O_{12}$-$Fe_3^{2+}Fe_2^{3+}Si_3O_{12}$, (almandine-"skiagite") and $Ca_3Fe_2^{3+}Si_3O_{12}$-$Fe_3^{2+}Fe_2^{3+}Si_3O_{12}$ (andradite-"skiagite") garnet solid solutions. Physics and Chemistry of Minerals, 21(3), 117-132.

Zhang, H.L., and Hirschmann, M.M. (in prep.) $Fe^{3+}/\Sigma Fe$ changes with pressure and its application to the early magma ocean.

Captions

Fig 1: Examples of Mössbauer spectra and their fits. a) M544 data collected at room temperature; b) M544 data collected at 67 K; c) VF3 data collected at room temperature; d) VF3 data collected at 67 K; e) VF3 data collected at room temperature fitted by assuming nanophase being Fe_3O_4; f) VF3 data collected at room temperature fitted by assuming nanophase being $MgFe_2O_4$. For all spectra, the pink curves refer to the paramagnetic Fe^{3+} doublets, the green curves refer to the paramagnetic Fe^{2+} doublets, and the blue curves are the superposition of all the sites. For e) and f), the orange curves refer to the superparamagnetic site.

Fig 2: Normalized absorption areas (AA) from M544 and VF3 Mössbauer spectra fit with xVBF methods as a function of temperature. Normalized area is the background-removed AA normalized by the AA at 47 K. a) and b) respectively show the normalized AAs for M544 and VF3 (normalized to AA at 47K). Dashed curves are normalized AA at 47 K from recoilless fractions calculated at different Debye temperatures.

Fig 3: Center shift (CS) from M544 and VF3 Mössbauer spectra fit with xVBF methods. a) and b) respectively show the CS changes with temperature in M544 and VF3. The blue curve, (Fe^{2+}) and green curves (Fe^{3+}), are fitted from Eqn. 3.

Fig 4: a) and b) respectively show $Fe^{3+}/\Sigma Fe$ ratios determined for M544 and VF3. The black squares refer to results obtained directly from uncorrected Mössbauer spectra. The red dots show $Fe^{3+}/\Sigma Fe$ ratios corrected by the relative method (RM), which is the recoilless fraction based on the Debye temperature obtained from the normalized area ratio changes with temperature, and the blue diamonds, refer to the $Fe^{3+}/\Sigma Fe$ ratios corrected by the recoilless fraction based on the Debye temperature obtained from the CS changes with temperature (CSM). For b), the orange star is the $Fe^{3+}/\Sigma Fe$ ratio determined by wet chemistry and electron microprobe.

720 Fig 5: a) and b) respectively show the hysteresis between applied magnetic field and sample
721 magnetization determined for M544 and VF3, both measured at 293 K. Orange curves refer
722 to the raw data and blue curves to the slope-corrected loop, derived from a regression line
723 subtracted through the outermost data points using the nonlinear high-field fitting at 70%.
724 Both slope-corrected curves saturate at high field intensity, indicating superparamagnetic
725 behavior.

726

727 Fig 6 Comparison of $Fe^{3+}/\Sigma Fe$ ratios for VF3 calculated with different methods with 2σ
728 uncertainties 1: Wet chemistry and Electron microprobe. 2: Uncorrected room temperature
729 Mössbauer spectra. 3: Room temperature Mössbauer spectra corrected with recoilless fraction
730 (f^{RM}) generated by the relative method (RM). 4: Uncorrected room temperature Mössbauer
731 spectra including a fit to the nanophase assumed to be pure $MgFe_2O_4$. 4.2: Uncorrected room
732 temperature Mössbauer spectra including a fit to the nanophase assumed to be pure Fe_3O_4. 5:
733 Room temperature Mössbauer spectra corrected with f^{RM} and including a fit to the nanophase
734 assumed to be pure $MgFe_2O_4$ and. 5.2: Room temperature Mössbauer spectra corrected with
735 f^{RM} and including a fit to the nanophase assumed to be pure Fe_3O_4 .

Figure 1a

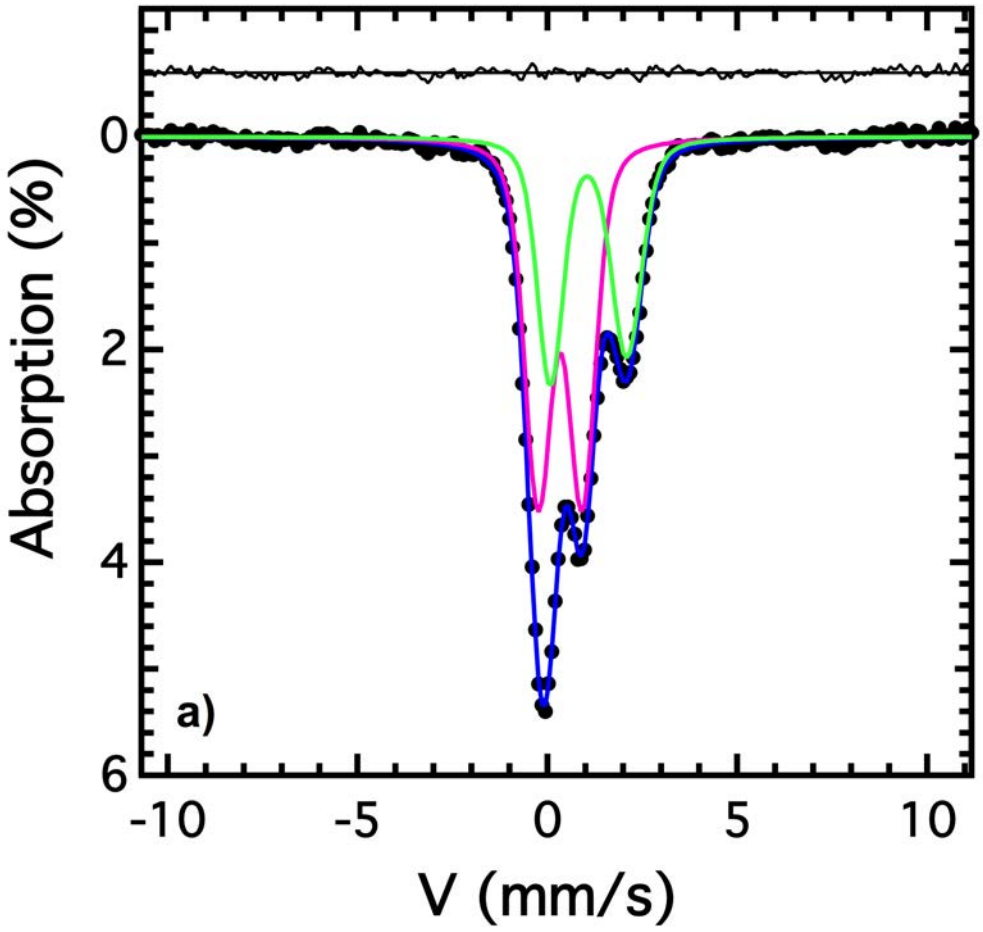

Figure 1b

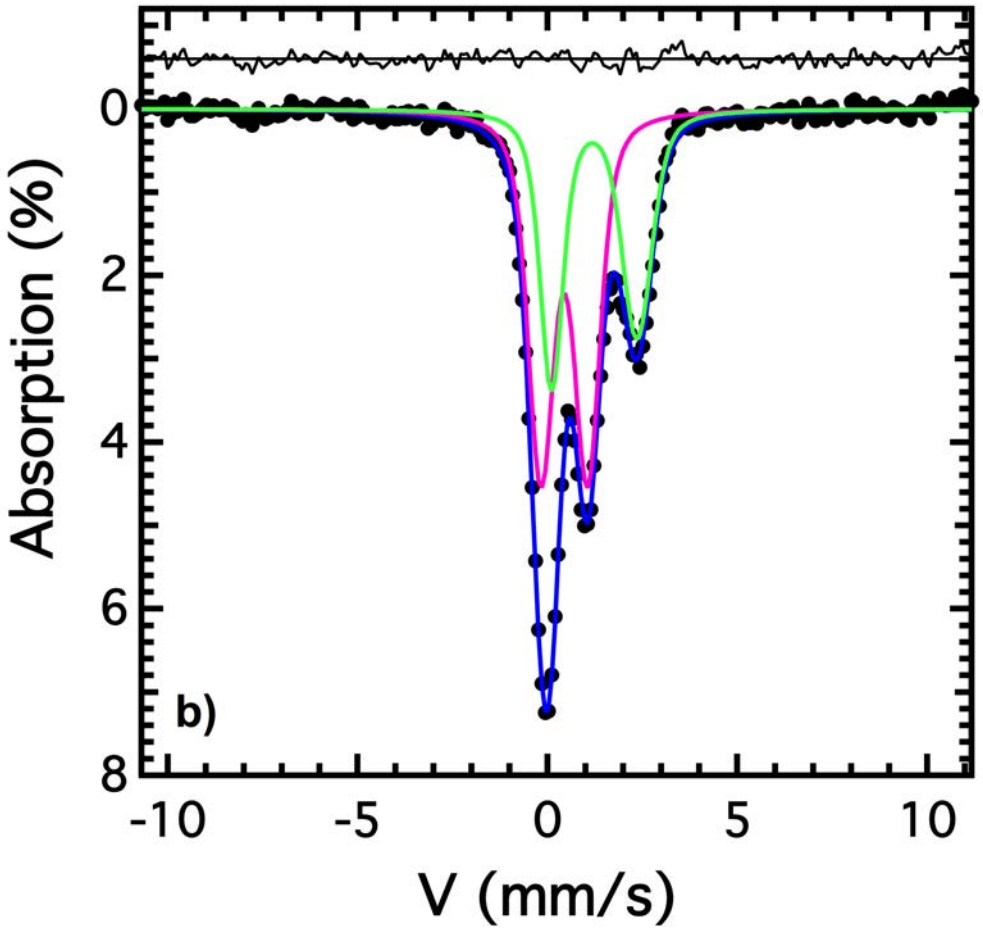

Figure 1c

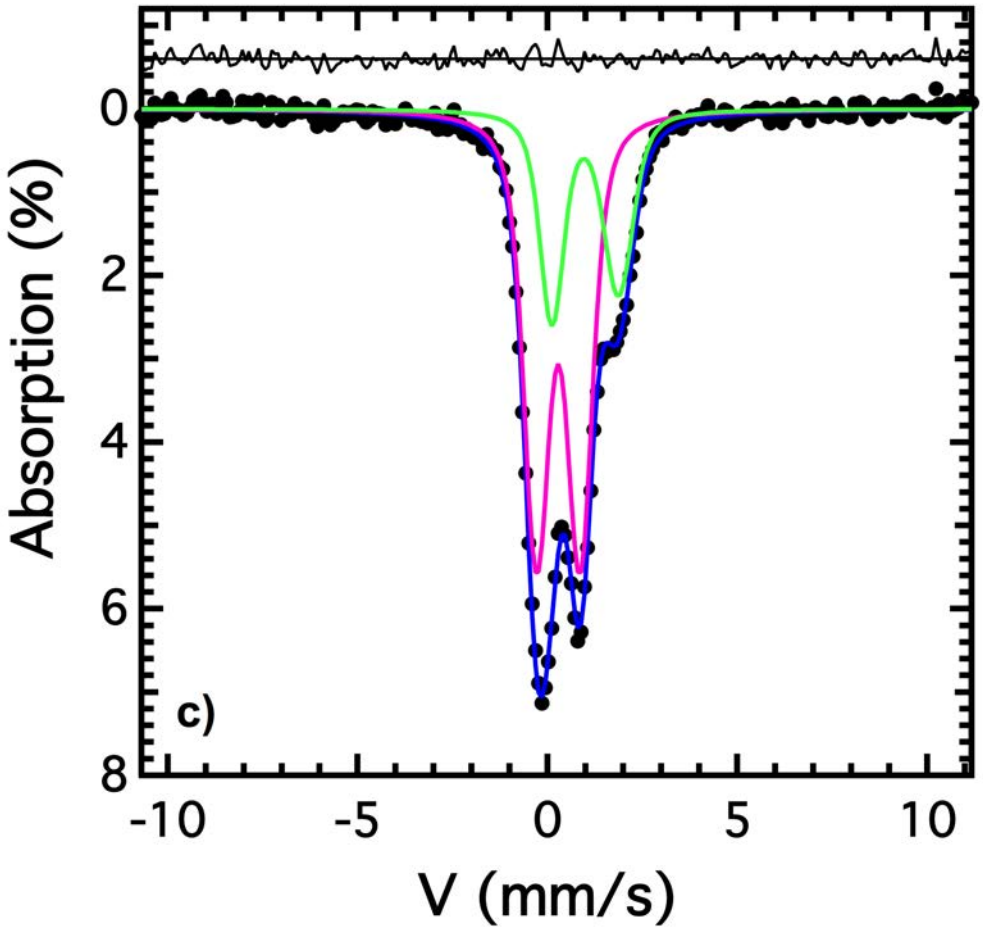

Figure 1d

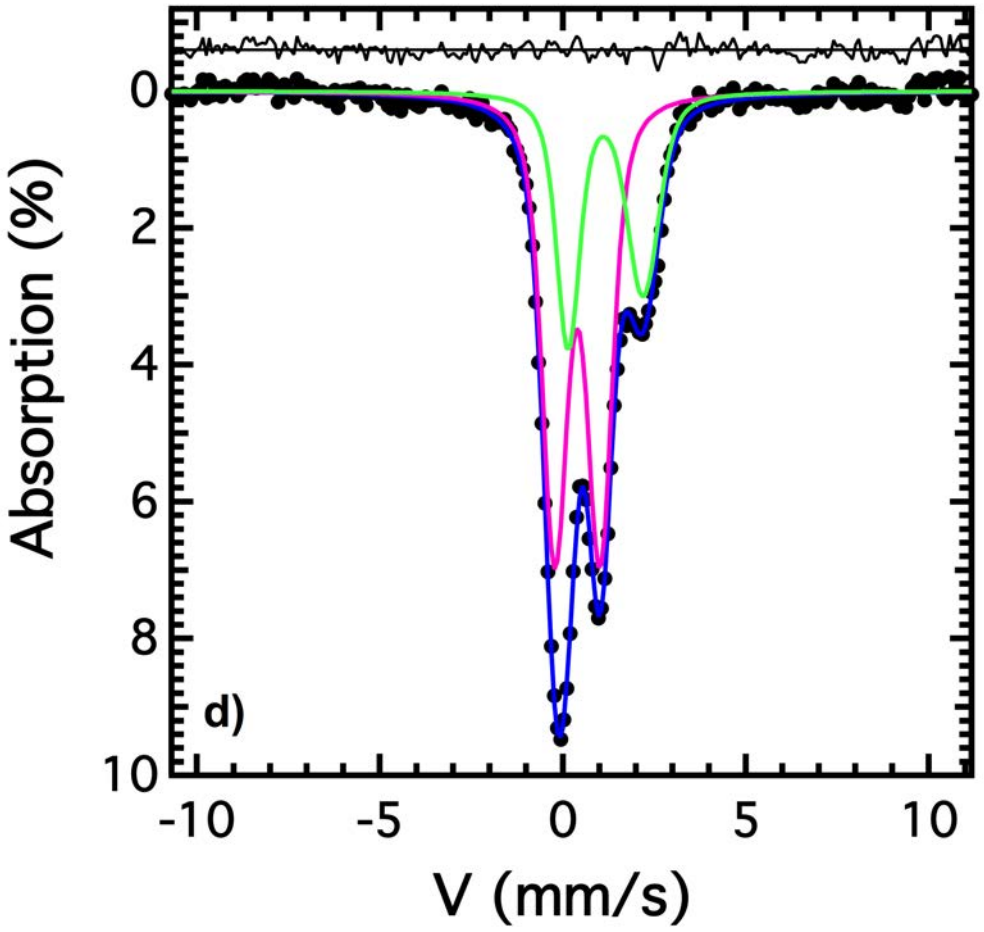

Figure 1e

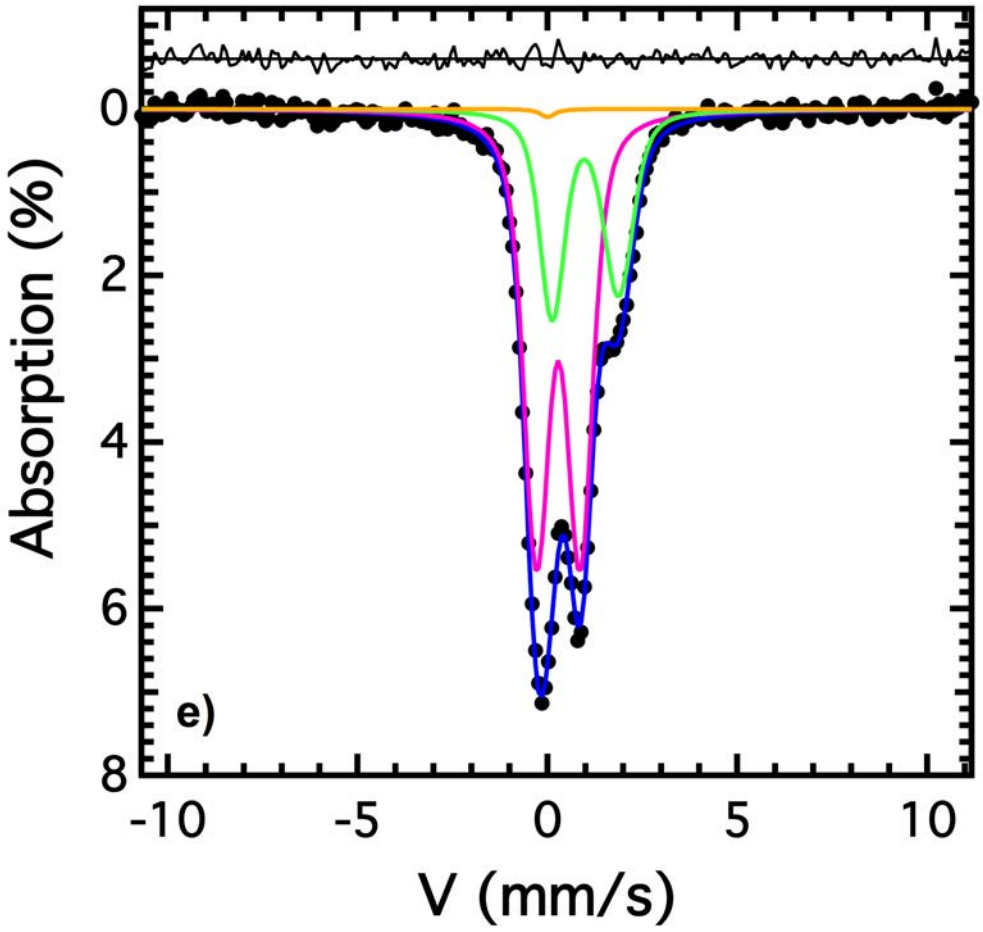

Figure 1f

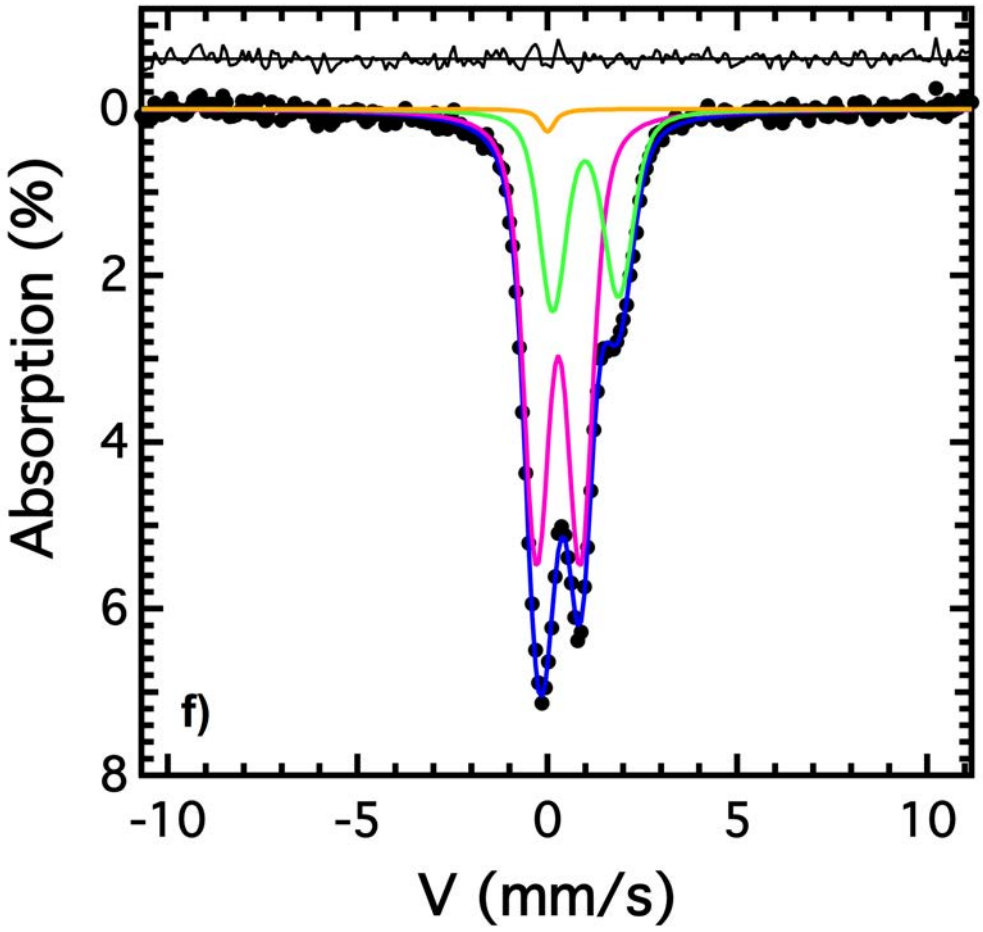

Figure 2a

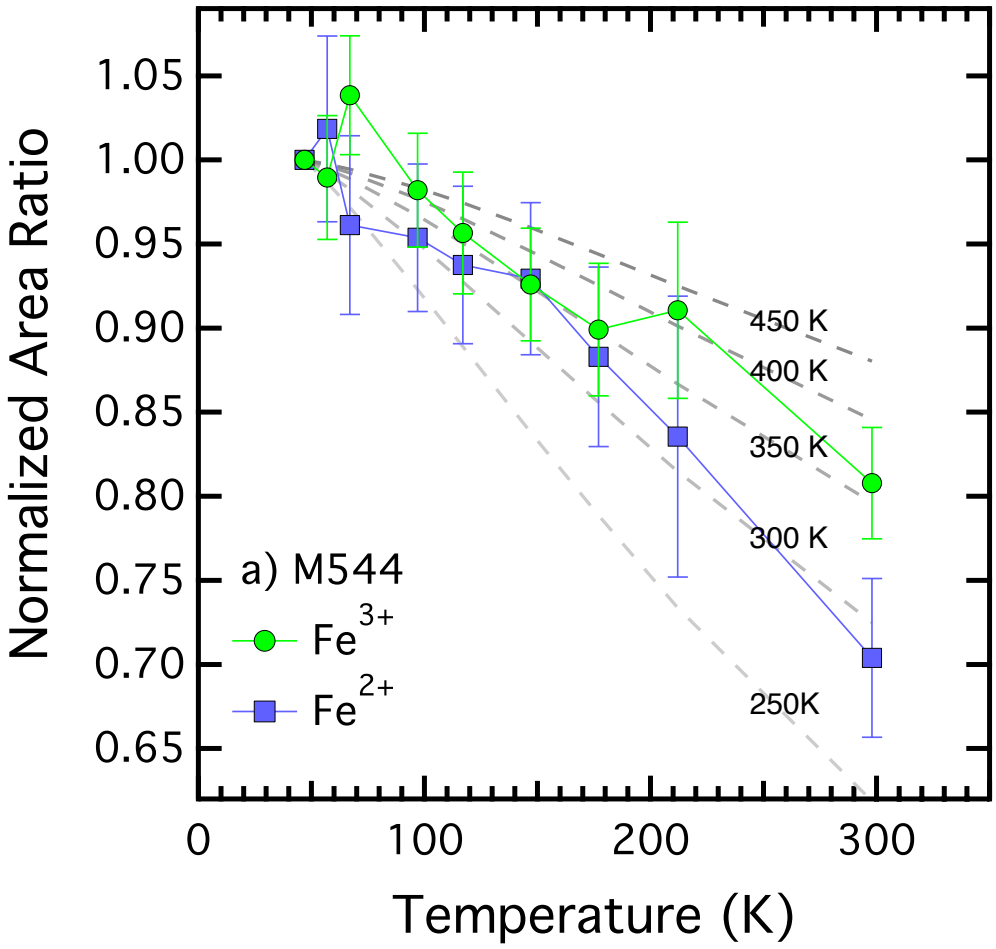
Normalized Area Ratio
1.05
1.00
0.95
0.90
0.85
0.80
0.75
0.70
0.65
0
100
200
300
Temperature (K)
a) M544
Fe3+
Fe2+
450 K
400 K
350 K
300 K
250K

Figure 2b

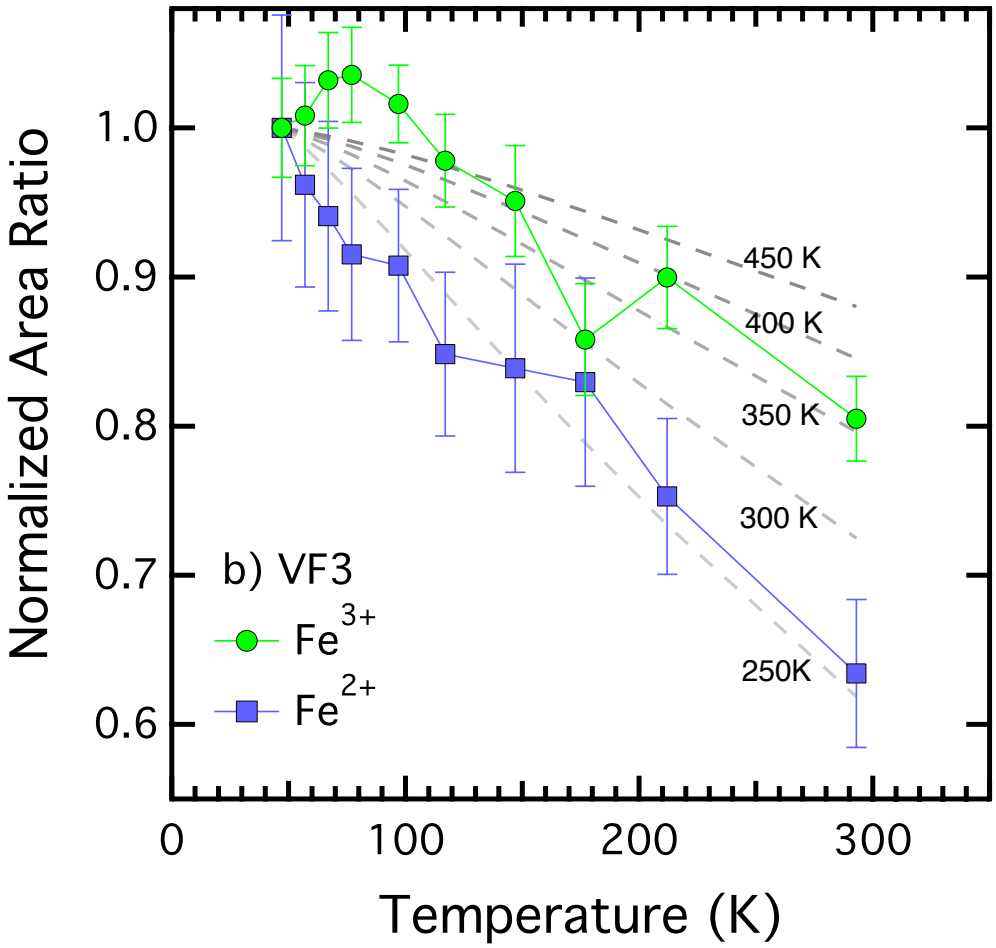
Normalized Area Ratio
1.0
0.9
0.8
0.7
0.6
0
100
200
300
Temperature (K)
b) VF3
Fe3+
Fe2+
450 K
400 K
350 K
300 K
250K

Figure 3a

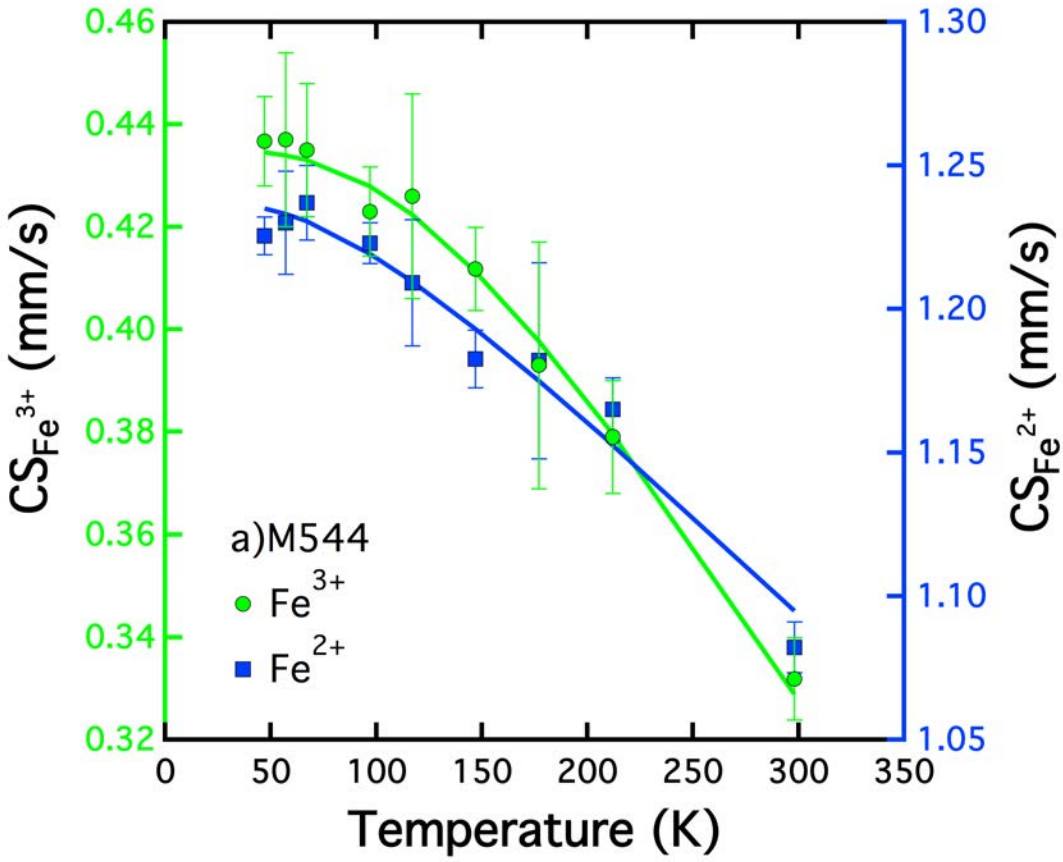
0.46
0.44
0.42
0.40
0.38
0.36
0.34
0.32
1.30
1.25
1.20
1.15
1.10
1.05
0
50
100
150
200
250
300
350
Temperature (K)
CS Fe3+ (mm/s)
CS Fe2+ (mm/s)
a)M544
Fe3+
Fe2+

This is a preprint, the final version is subject to change, of the American Mineralogist (MSA)
Cite as Authors (Year) Title. American Mineralogist, in press.
(DOI will not work until issue is live.) DOI: http://dx.doi.org/10.2138/am-2015-5161

Figure 3b

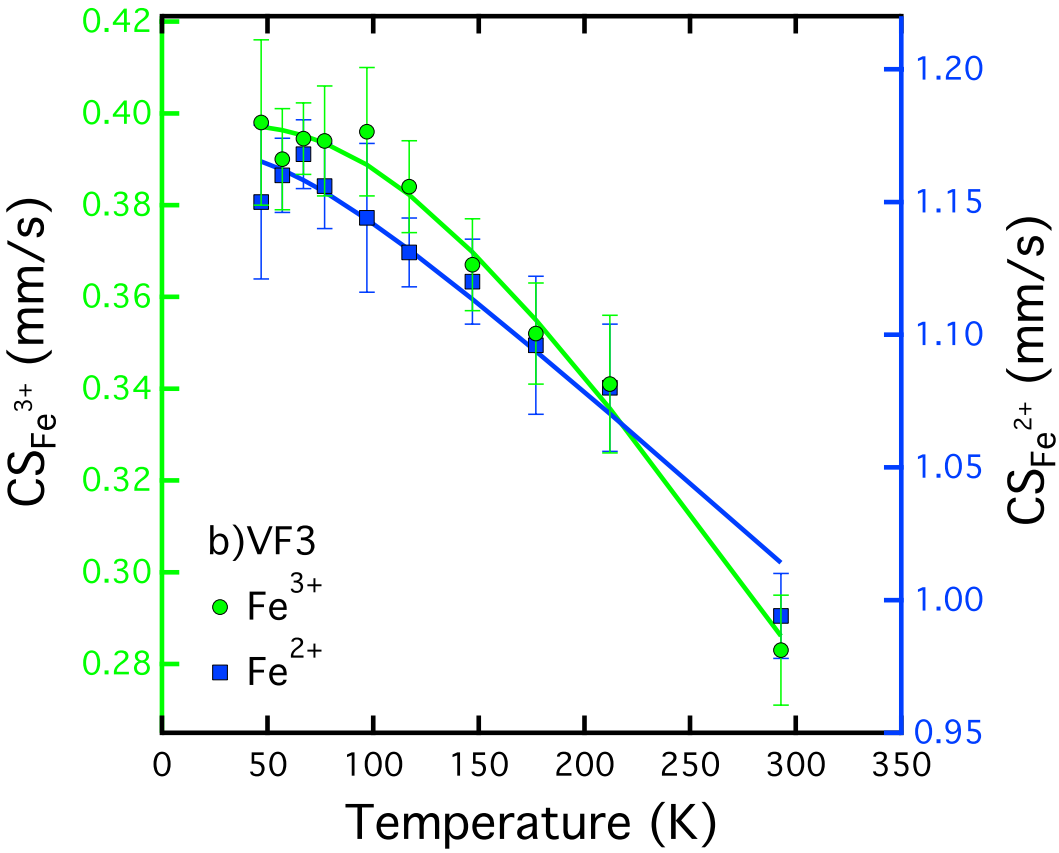

Figure 4a

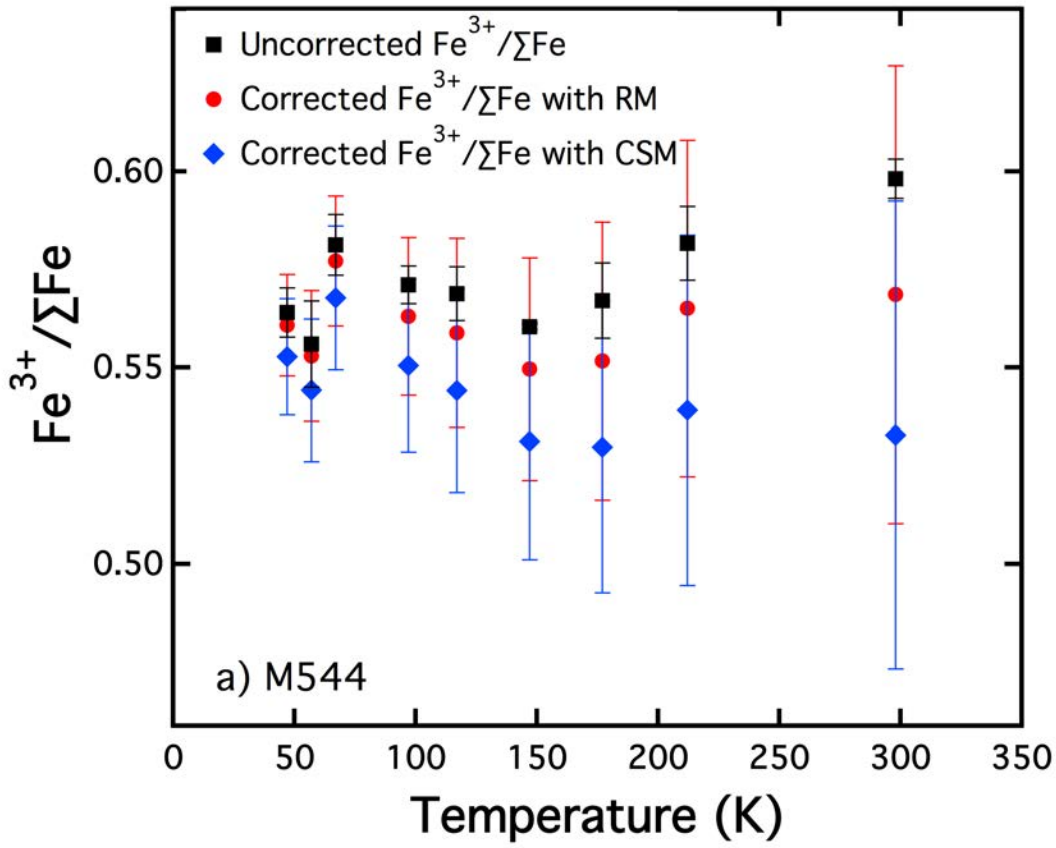

Figure 4b

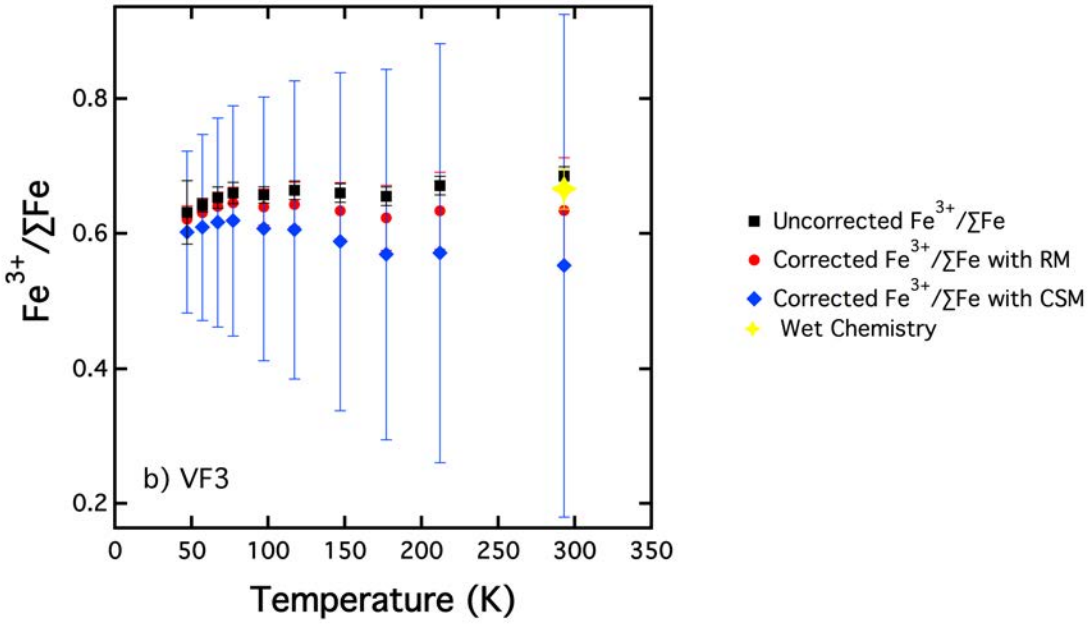

Figure 5a

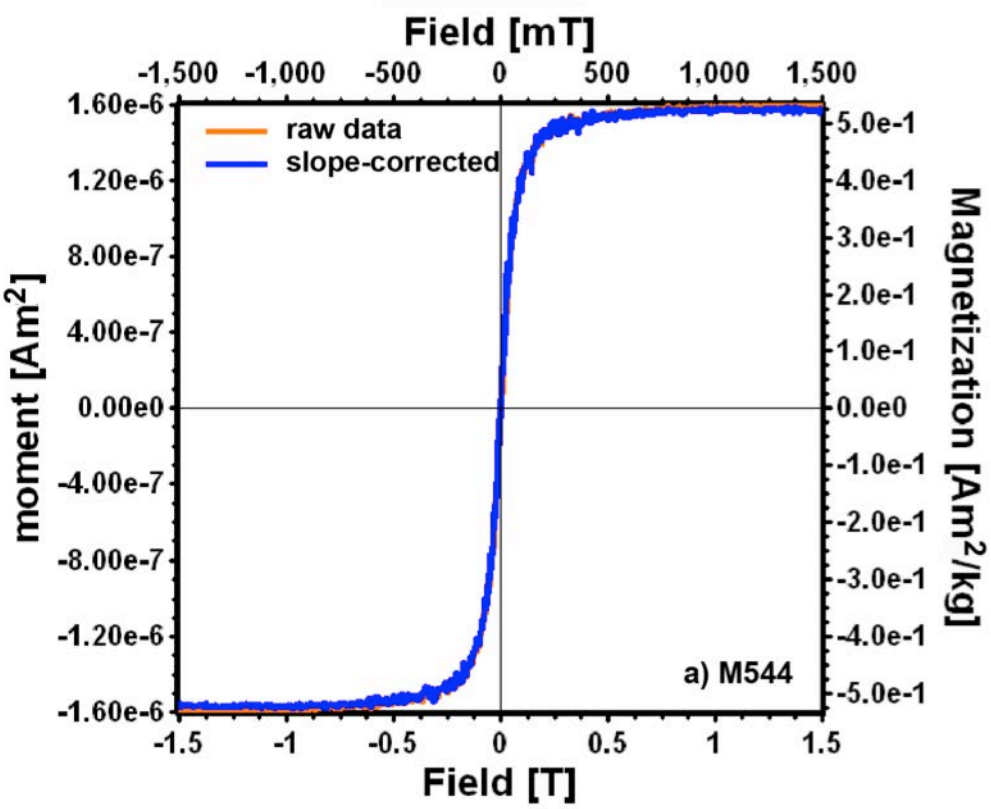

Figure 5b

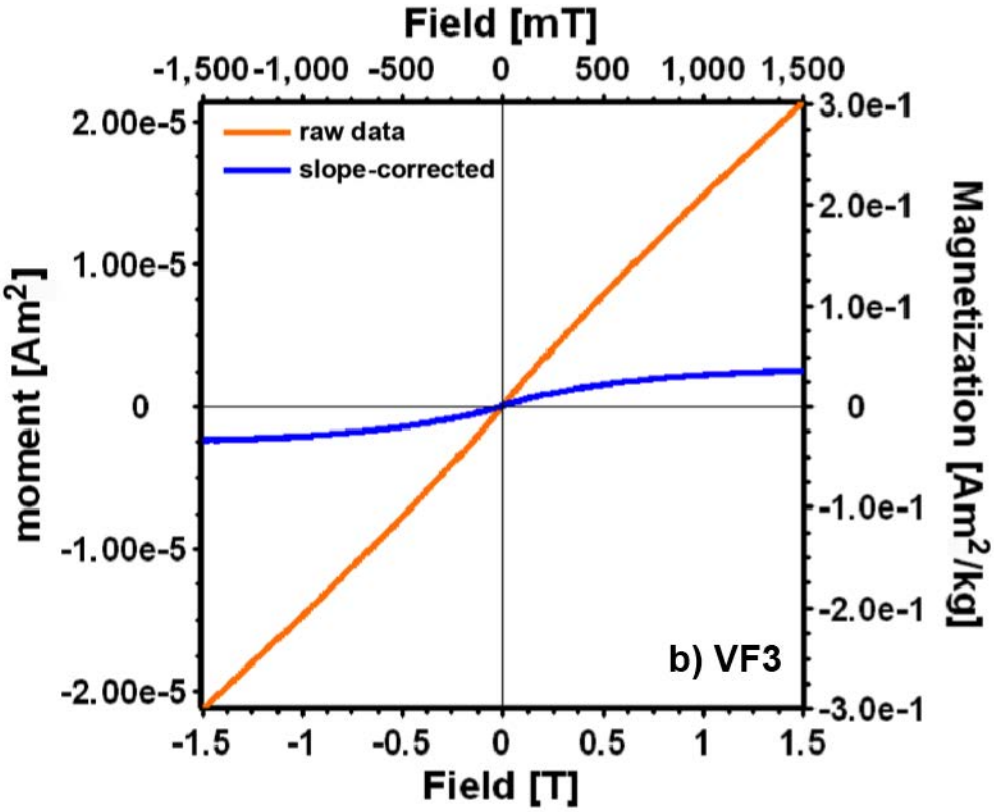

Figure 6

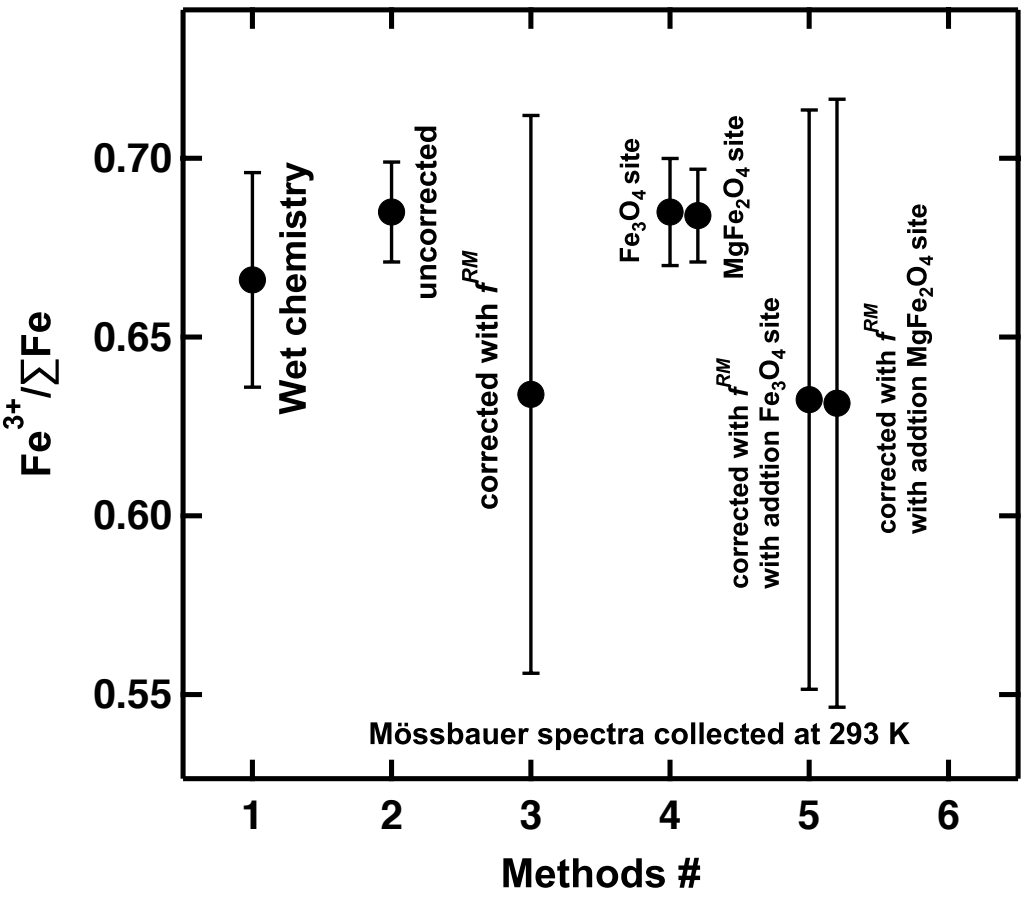
0.70
0.65
0.60
0.55
$Fe^{3+}/\sum Fe$
Wet chemistry
uncorrected
corrected with f^{RM}
Fe_3O_4 site
$MgFe_2O_4$ site
corrected with f^{RM} with addtion Fe_3O_4 site
corrected with f^{RM} with addtion $MgFe_2O_4$ site
Mössbauer spectra collected at 293 K
1
2
3
4
5
6
Methods #

This is a preprint, the final version is subject to change, of the American Mineralogist (MSA)
Cite as Authors (Year) Title. American Mineralogist, in press.
(DOI will not work until issue is live.) DOI: http://dx.doi.org/10.2138/am-2015-5161

Table 1:Electron microprobe analyses of sample and standard glasses

	ATHO-G(11)[1]	ATHO-G[r]	BCR-2G(9)[1]	BCR-2G[r]	BIR-1G(9)[1]	BIR-1G[r]	VF3(10)[1]	M544(8)[1]
SiO_2	75.50±0.92	75.60±1.40	54.35±0.74	54.40±0.80	47.32±0.74	47.50±0.60	56.89±1.38	57.89±1.76
TiO_2	0.24±0.08	0.255±0.032	2.16±0.26	2.27±0.08	0.90±0.12	1.04±0.14	2.80±0.16	2.68±0.12
Al_2O_3	12.10±0.26	12.20±0.40	13.31±0.24	13.40±0.80	15.45±0.20	15.50±0.40	14.89±0.38	15.09±0.64
FeO*	**3.28±0.10**	**3.27±0.20**	**12.50±0.36**	**12.50±0.60**	**10.37±0.14**	**10.40±0.20**	**9.29±0.22**	**8.92±0.12**
MnO	0.10±0.02	0.11±0.010	0.20±0.02	0.19±0.02	0.17±0.04	0.19±0.02	0.06±0.02	0.03±0.04
MgO	0.11±0.02	0.10±0.02	3.73±0.18	3.56±0.18	9.95±0.22	9.40±0.20	2.26±0.08	2.24±0.08
CaO	1.78±0.04	1.70±0.06	7.20±0.12	7.06±0.22	13.39±0.24	13.30±0.40	7.60±0.10	7.40±0.08
Na_2O	3.63±0.40	3.75±0.62	3.05±0.36	3.23±0.14	1.76±0.16	1.85±0.14	4.21±0.32	4.34±0.12
K_2O	2.72±0.08	2.64±0.18	1.78±0.08	1.74±0.08	0.02±0.02	0.03±0.010	1.06±0.06	1.06±0.02
Total	99.46	99.62	98.27	98.35	99.33	99.21	99.06	99.65

Notes: 1:Electron microprobe analyses. Number in parentheses indicates the number of analyses averaged.
r:BIR-1G and BCR-2G reference values from Jochum et al. (2005) and ATHO-G reference values from Jochum et al. (2006). FeO*:Total Iron contents. All uncertainties are in two sigma range standard deviation (2σ)

Table 2: Wet chemical determinations of FeO

		Measured	Accepted
USGS standards	QL	2.84	2.97[#]
	W-2a	8.1	8.34[#]
Replicates			
	VF3	2.9	
	VF3	2.99	
	VF3	3.03	
	VF3	3.02	
	Average VF3	2.99	3.10[##]±0.24[####]
	$Fe^{3+}/\Sigma Fe$		0.666[###]±0.030[####]

Notes: #: QL and W-2a reference values from Govindaraju(1994).□##: Average VF3 value corrected accounting for the bias in the analyses of the USGS standards. ###: $Fe^{3+}/\Sigma Fe$ calculated from FeO*= 9.29 wt% (Table1). ####: Uncertainties are in two sigma range standard deviation (2σ)